MULTI-FREQUENCY GROUND-PENETRATING RADAR (GPR) STUDY OF GLACIOFLUVIAL OUTWASH DEPOSITS, LIMEHOUSE, ONTARIO

MULTI-FREQUENCY GROUND-PENETRATING RADAR (GPR) STUDY OF GLACIOFLUVIAL OUTWASH DEPOSITS, LIMEHOUSE, ONTARIO

By

NICOLE K. FALLON, B.Sc. (Hons)

A Thesis

Submitted to the School of Graduate Studies

in Partial Fulfillment of the Requirements

for the Degree

Master of Science

McMaster University

MASTER OF SCIENCE (2012)	McMaster University
Geography and Earth Sciences	Hamilton, Ontario
TITLE:	**Multi-frequency Ground-Penetrating Radar (GPR) Study of Glaciofluvial Outwash Deposits, Limehouse, Ontario**
AUTHOR:	Nicole K. Fallon, B.Sc (Hons) (McMaster University, Hamilton, 2009)
SUPERVISOR:	Professor J. I. Boyce
NUMBER OF PAGES:	x, 128

ABSTRACT

In this study, the spatial trends in heterogeneity and sedimentary architecture of a coarse-grained glaciofluvial deposit were investigated in a gravel pit near Limehouse, Ontario using multi-frequency ground-penetrating radar (GPR). The well-exposed outcrops in the pit (> 10 m) allow direct comparison of radar and outcrop lithofacies and provide 'outcrop analogues' for regional glaciofluvial aquifers present in the shallow subsurface. GPR surveys were acquired using four different frequencies (25, 50, 100 and 250 MHz) over a 5800 m^2 grid on the pit floor and along an adjacent outcrop and roadway. Profiles were acquired at 2 m line spacing using D-GPS positioning and processed to a quasi-3D volume in GPR-SLICE software.

Radar reflection patterns were grouped into radar facies and interpreted using architectural element analysis (AEA) with reference to outcrops and a nearby geophysically logged borehole (MW-22). Using this approach, five distinctive lithosomes and two depositional phases were identified. The lithosomes consist of gravel clinoform (GC) elements, gravel bar (GB) and gravel foreset (GF) elements, vertical aggradation (VA) elements and incised channel elements (CH). RP-1 (elements GC, CH, GB) records the progradation of a sub-aqueous fan delta into a shallow proglacial lake. RP-2 records a subsequent phase of incision of deltaic deposits by glaciofluvial spillways and infilling of channels by aggradation of braided river sand and gravel deposits.

Comparison of the radar profiles with borehole and outcrop data indicates that lithosome bounding surfaces are associated with major changes in sediment texture. Lithosomes defined using radar reflection patterns can therefore be used to predict changes in sediment grain size and associated hydrogeologic parameters (e.g. hydraulic conductivity). These results demonstrate that multi-frequency GPR is a viable approach for evaluating spatial trends in sedimentary heterogeneity and can be applied at other sites under consideration for artificial recharge projects.

ACKNOWLEDGEMENTS

Endless gratitude goes to my supervisor Dr. Joe Boyce for giving me the opportunity to complete this project and guiding me through the research process. Working with you gave me invaluable experience and knowledge that I will carry with me for the rest of my life. Many thanks also extend to Dr. Carolyn Eyles, who has been a great help over the last few years. Also, this project would not have been possible without the funding and support of Tim Lotimer and the Regional Municipality of Halton.

This project would not have been completed without Andrew Brennan and Peter Dao. Not only are you the best field ‘helpers’ around, but the many beverages, many laughs, many ninja jokes and many quotes of the day helped keep me sane thought it all. I could never buy enough coffees of the day to show my appreciation for everything. I would also like to thank Stacey Puckering, Jessica Slomka, Paul Durkin, Riley Mulligan, Phil Suttak and Prateek Gupta for their help with field work and everything else over the last couple of years.

I thank my friends and family for their tireless support, and I sincerely thank Mark for taking such a keen interest in rocks. Last but not least, to my parents; none of this would have been accomplished without your continual encouragement. I am where I am because of you and I could not appreciate you more.

TABLE OF CONTENTS

LIST OF FIGURES AND TABLES

CHAPTER 1: INTRODUCTION

1.1 BACKGROUND AND RATIONALE

In Ontario, Canada over 3.8 million residents rely on groundwater for domestic uses (Fig. 1.1a). As Ontario's population continues to grow to an anticipated 15 million by 2025, the demands for groundwater will increase (Holysh, 1995). The pressures will likely be greatest in communities surrounding the rapidly urbanizing Greater Toronto Area (GTA) where development is placing an increasing demand for groundwater (Meyer and Eyles, 2007; Brennan, 2011). The expansion of urban areas into sensitive groundwater recharge areas (e.g. the Oak Ridges Moraine) is also impacting groundwater quality and quantity (Howard et al., 1995).

In the Regional Municipality of Halton (HR), located in the western GTA (Fig 1.1a) about 30% of the region's residents are currently dependent on groundwater from municipal or private wells (Holysh, 1995). Within Halton Hills (towns of Georgetown and Acton), more than 40,000 people utilize groundwater for both residential and commercial use. HR has taken a proactive approach to groundwater management by developing a comprehensive aquifer management plan and wellhead protection program (Holysh, 1995). Aquaresource (2008) found that even at current population levels watersheds in the area are under moderate stress due to reductions in baseflow to streams and degradation of stream water quality. As well, the region is still experiencing difficulty locating new, sustainable groundwater sources, which has lead to restrictions

Figure 1.1: A. Surficial geology of southern Ontario showing location of study site. B. Georgetown area showing location of Niagara Escarpment, buried bedrock channels and glaciofluvial spillway systems. Paleoflow directions also shown. C. Laurentide Ice Sheet (LIS) during its maximum extent over southern Ontario (ca. 22-16 Ka BP). D. Formation of Oak Ridges interlobate moraine between the Simcoe and Ontario lobes during LIS retreat (ca.13 Ka BP). The Limehouse glaciofluvial deposits were formed in a proglacial setting during the interstadial period or during the final readvance of Ontario lobe (modified from Slomka, 2011).

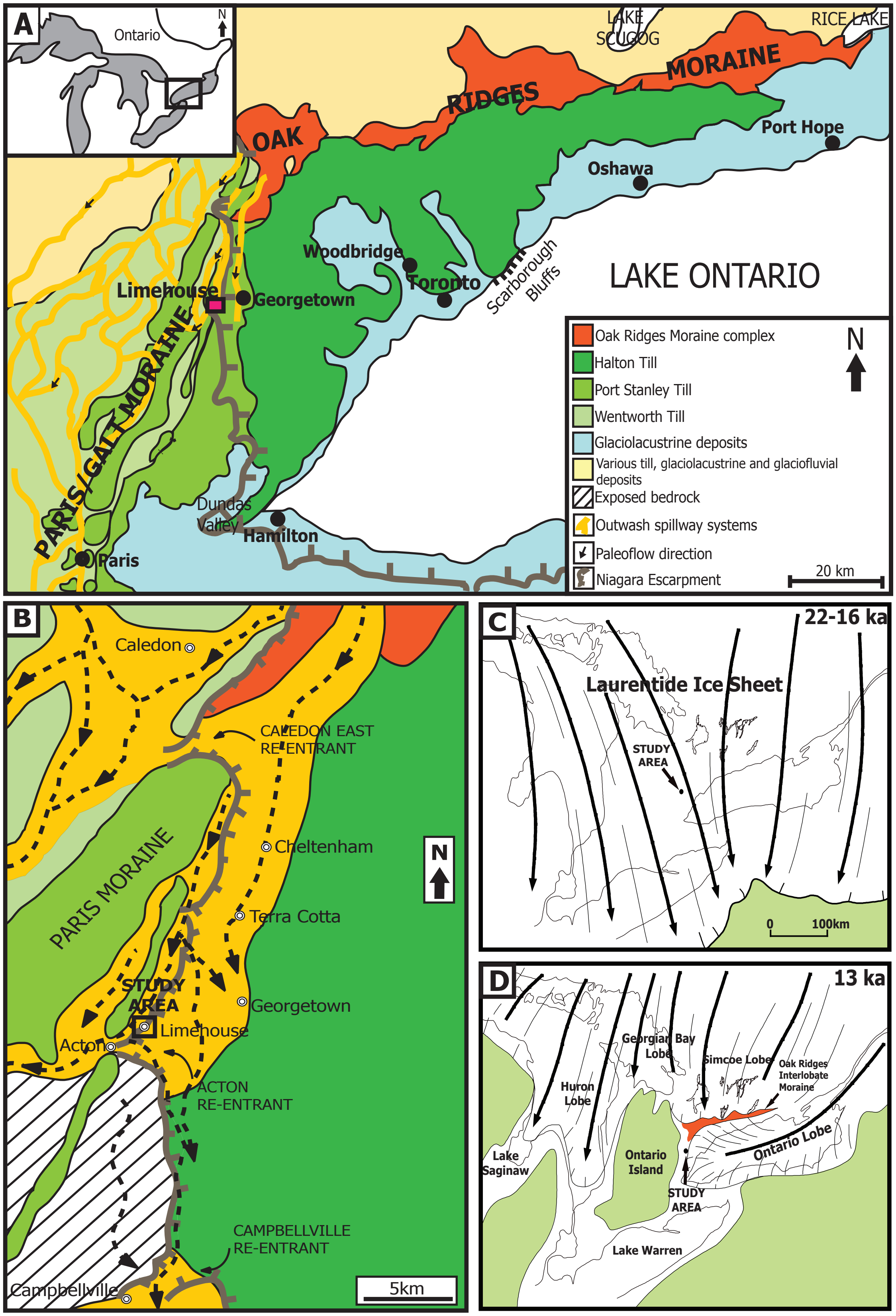
A
Ontario
N
LAKE SCUGOG
RICE LAKE
OAK RIDGES MORAINE
Port Hope
Oshawa
Woodbridge
Toronto
Scarborough Bluffs
LAKE ONTARIO
Limehouse
Georgetown
PARIS/GALT MORAINE
Dundas Valley
Hamilton
Paris
Oak Ridges Moraine complex
Halton Till
Port Stanley Till
Wentworth Till
Glaciolacustrine deposits
Various till, glaciolacustrine and glaciofluvial deposits
Exposed bedrock
Outwash spillway systems
Paleoflow direction
Niagara Escarpment
20 km
B
Caledon
CALEDON EAST RE-ENTRANT
Cheltenham
Terra Cotta
PARIS MORAINE
STUDY AREA
Georgetown
Limehouse
Acton
ACTON RE-ENTRANT
CAMPBELLVILLE RE-ENTRANT
Campbellville
5km
C
22-16 ka
Laurentide Ice Sheet
STUDY AREA
0 100km
D
13 ka
Georgian Bay Lobe
Simcoe Lobe
Oak Ridges Interlobate Moraine
Huron Lobe
Ontario Lobe
Lake Saginaw
Ontario Island
STUDY AREA
Lake Warren

on development in the region. The problems locating potential aquifers come mainly from a lack of understanding of the extent, thickness and geometry of high yielding Quaternary deposits (Holysh, 1995). In order to identify areas that may be suitable for use as sources of clean groundwater, these undefined areas need to be modeled and understood.

In 2008, HR and McMaster University initiated a 2-year collaborative study of the Quaternary geology and hydrostratigraphy of the Georgetown area. One of the aims of the project was to better understand the sedimentary characteristics and 3-dimensional geometry of Quaternary sediments that infill several buried valleys below Georgetown area (Fig. 1.1b) (Brennan, 2011; Slomka, 2011). The Quaternary sediments reach a thickness of over 50 m and include thick sand and gravel units that are capable of supplying high yield municipal wells (Meyer and Eyles, 2007). The lateral extent and continuity of coarse-grained aquifers and intervening aquifers units, however, is not well understood and is a major obstacle to groundwater exploration. In order to address these knowledge gaps, a program of surface geophysics (seismic, ground-penetrating radar) and drilling of continuously-cored boreholes was conducted at several locations around Georgetown to provide new, high-quality subsurface information.

Because of the current shortfall in groundwater supply, HR is also investigating the feasibility of artificial recharge of existing aquifers using surface waters. Artificial recharge is a means of replenishing groundwater by putting water on or in the ground and allowing it to infiltrate the soil and recharge aquifers. In areas where the subsurface is made up of permeable materials, the water can permeate through the sediment and into underlying aquifers. In cases where cases highly permeable surficial sediments are not present, water can be injected into the aquifers through wells, trenches or shafts excavated in the unsaturated zone (Freeze and Cherry, 1979). The water for artificial recharge can come from streams regulated with dams, storm runoff, aqueducts and water treatment plants (both drinking water and sewage).

Several potential artificial recharge sites have been identified in HR where aquifers could be replenished via infiltration of surface waters. These include a number of existing aggregate pits situated within thick glaciofluvial sand and gravel deposits. These sites could provide favourable conditions for direct recharge of local and regional aquifers but the subsurface geology and geometry of the glaciofluvial deposits is not yet well understood. An objective of this study was to better resolve the 3-dimensional sedimentary variability and geometry of surficial glaciofluvial deposits exposed in gravel pits to the northwest of Georgetown (see 1.2.4 below).

The hydraulic properties of glaciofluvial aquifers are controlled to a large extent by their sedimentary characteristics, including sediment texture, thickness, lateral extent and geometry (Asprion and Aigner, 1997). The sedimentary heterogeneity of glaciofluvial aquifers is often complex and can lead to large uncertainties in predicting groundwater flow and contaminant migration in the subsurface (Beres et al. 1999). A major problem is that most facies models used to describe glaciofluvial aquifers are based on one- or two-dimensional data from outcrop exposures (Anderson, 1989) and often lack the necessary data for construction of 3-dimensional subsurface models. An approach that is employed increasingly is to combine outcrop analysis with 2- and 3-dimensional ground-penetrating radar (GPR) surveys (Goutaland et al., 2008).

GPR was chosen for this study because it has been employed elsewhere with great success in coarse-grained deposits, including glaciofluvial sediments (Van Overmeeren, 1998; Martinez et al. 1999; Jol, Lawton and Smith, 2002; Xia et al. 2004; Bersezio, Giudici and Mele, 2007). Initially, GPR was utilized mainly in hydrocarbon and aquifer studies, as the reflection profiles readily show the primary structure of subsurface sediments (Neal, 2004). More recently, it has proven useful in a number of hydrostratigraphic studies conducted worldwide and in a variety of geological settings, including glaciofluvial deposits.

Quarries are excellent sites for GPR surveys of glaciofluvial deposits, as the sediments are well exposed in the pit walls, allowing for direct comparison of radargrams with outcrop lithofacies. Many such studies have been completed in Switzerland (Huggenberger, 1993; Beres et al. 1999) and Germany (Asprion and Aigner, 1997; Asprion and Aigner, 1999; Heinz et al. 2003; Kostic and Aigner, 2007). These studies have shown that the geometry of sedimentary facies observed in radargrams and outcrops are often similar, but some units identified in outcrop may remain undetected due to resolution problems (Kostic and Aigner, 2007). A common finding in these studies is that glaciofluvial deposits display a very high degree of spatial complexity and heterogeneity that is difficult to characterize with outcrops alone because lateral information is unavailable when solely outcrop information is available. The 3-dimensional information proves extremely useful for predicting preferential flow pathways, which determine how and where groundwater can flow (Lesmes et al. 2002; Bowling et al. 2005; Kostic and Aigner, 2007).

A number of GPR studies have employed architectural element analysis (AEA) as an approach for interpretation of radargrams. AEA recognizes that many areas have a high degree of lateral variability and that the geometry of lithosomes is complex (Boyce and Eyles, 2000). Kostic and Aigner (2007) used GPR and AEA (termed depositional element analysis) to characterize the sedimentary architecture of coarse-grained river deposits and reconstruct their three-dimensional internal architecture. They then linked the sediment architecture to the hydrogeology of valley aquifers. Using a classification system similar to that of Miall (1985), they defined five lithofacies classes within their outcrop and GPR profiles. They used both the geometries of the major reflection terminations and internal reflection configurations to identify the depositional elements. They acknowledge that by understanding the sedimentary architecture they were able to gain a better insight into the groundwater flow. Similarly, Boyce and Eyles (2000) utilized AEA in conjunction with outcrop and well log data to create a three-dimensional subsurface model of an extensive till sheet for the purposes of evaluating the its hydrogeological properties. They too concluded that AEA was highly useful for both understanding the origins of bedforms and subglacial processes and as a basis for understanding flow pathways for groundwater and contaminants.

1.2 STUDY AREA

1.2.1 Site Location

GPR surveys were conducted in a gravel pit near the town of Limehouse, Ontario (Fig. 1.1b). The Limehouse quarry includes two active pits, the Wilroy Pit and the Bot Duff Pit (Fig. 1.2), located on the 4th Line about 2 km northwest of Limehouse. The quarries were opened in 1965 and have been in use for aggregate extraction since then.

This study focuses on the Wilroy Pit, which is approximately $0.24km^2$. The pit has a 300 m long outcrop face running along the east side of the pit, which exposes mainly gravels and coarse sands. A geophysically logged borehole (MW-22) is located 100 m northeast of the pit on 4th Line (Fig.1. 2).

1.2.2 Bedrock Geology

The bedrock beneath the study area consists of Paleozoic-age clastic and carbonate rocks deposited on the margins of the Michigan basin (Karrow, 1984). In the Georgetown area, to west of the Niagara Escarpment, bedrock consists of Ordovician (Queenston Formation) red shales and siltstones. The shales are typically heavily weathered and are overlain by a variable thickness of shale regolith (head unit). In the vicinity of the Niagara Escarpment the Queenston shales are overlain by interbedded sandstone, shale and dolostone of the Clinton-Cataract Group. These sediments are exposed locally in stream cuts and in limited outcrops at the base of the Niagara

Figure 1.2: Aerial photo of Wilroy and Duff-Bott pits showing location of 3-D GPR survey Grids (1 and 2) and 2-D radar profiles. The pit stratigraphy is well exposed in a 12 m high outcrop located on the northeast wall of the pit. Location of MW-22 monitoring well also shown.

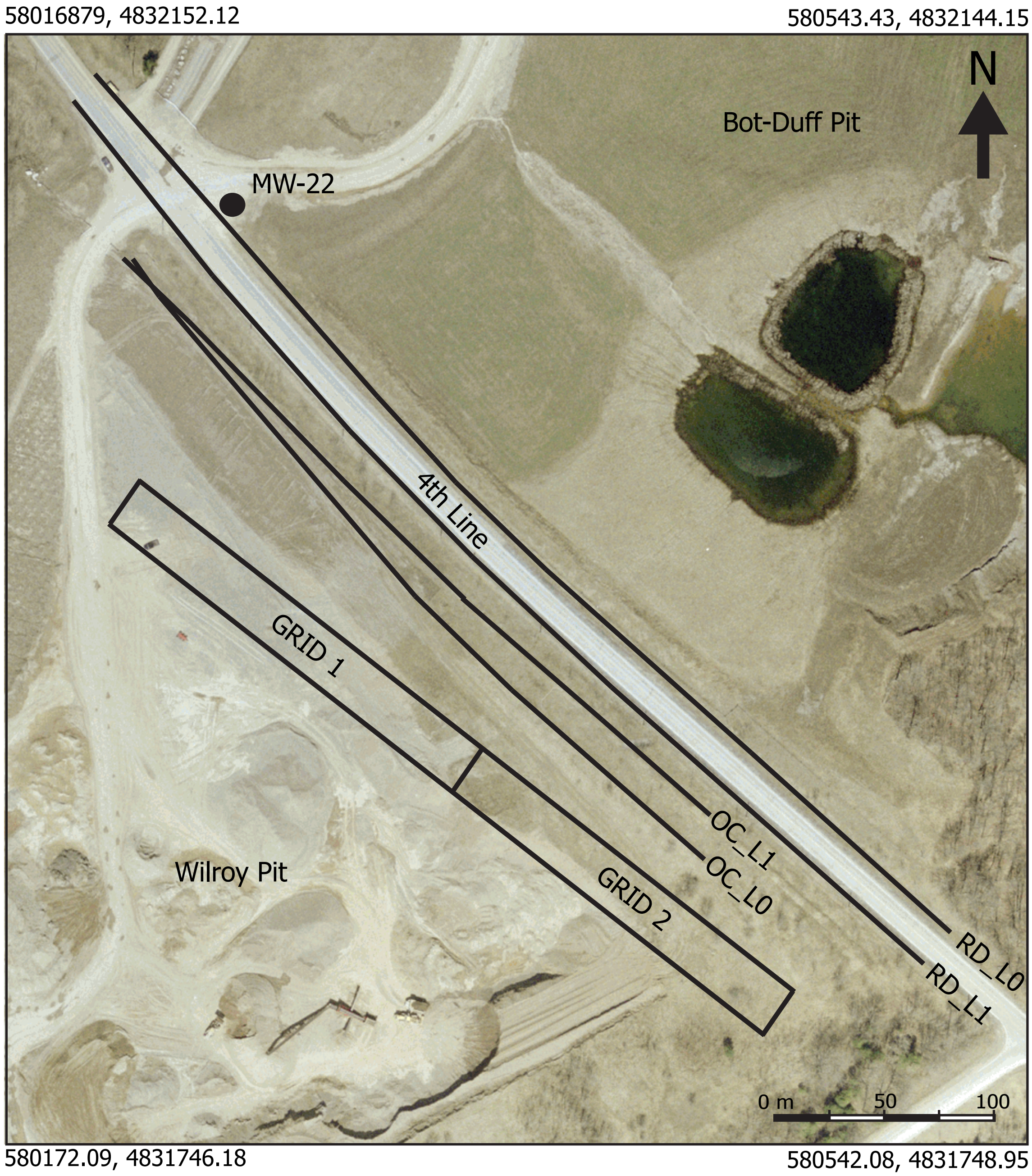
58016879, 4832152.12
580543.43, 4832144.15
N
Bot-Duff Pit
MW-22
4th Line
GRID 1
GRID 2
OC_L1
OC_L0
RD_L0
RD_L1
Wilroy Pit
0 m
50
100
580172.09, 4831746.18
580542.08, 4831748.95

Escarpment. The Clinton-Cataract Group is in turn overlain by the Lockport Formation dolostones, which form the resistant cap rocks of the Niagara Escarpment. The Lockport dolostones are exposed at surface near Limehouse in an outlier formed at the eastern end of the Acton re-entrant valley (Fig. 1.1b). Bedrock is not exposed in the Wilroy or Bot-Duff pits but the nearby borehole MW-22 (Fig. 1.2), which indicates that the bedrock surface is about 12 m below the pit base. Based on its elevation the bedrock beneath the site is most likely the Lockport Formation dolostones.

1.2.3 Quaternary Geology

The predominant surficial sediments across southern Ontario are Quaternary sediments deposited during multiple advances and retreats of the Laurentide Ice Sheet (LIS) (Barnett, 1992). In Halton Region, Quaternary deposits reach more than 75 m in thickness within a number of broad buried bedrock valleys (Meyer and Eyles, 2007; Puckering, 2011). The buried valley stratigraphy includes two regionally extensive Late Wisconsin till sheets (Halton and Newmarket tills) and intervening coarse-grained sand and gravels deposited during a brief interstadial period (Mackinaw Interstadial) (Karrow, 1984; Barnett 1992; Meyer and Eyles, 2007). The coarse-grained interstadial deposits are of regional hydrogeologic importance because they host shallow aquifers capable of sustaining municipal wells (Holysh, 1995) and could provide potential artificial recharge sites where they are locally in direct hydraulic communication with underlying deeper aquifers (Brennan, 2011).

1.2.4 Previous work

The Quaternary surficial and subsurface geology of the study area has been investigated in a number of previous studies. Karrow (1967) mapped the Quaternary surficial geology of Halton and identified two regional till sheets and associated glaciofluvial outwash deposits. The lowermost till is a sandy, overconsolidated diamict present in the subsurface across most of HR. Locally, the till has been truncated by younger glaciofluvial sediments and is absent in the subsurface (Brennan, 2011). The age of this till unit is not clear but based on its stratigraphic position and its characteristic well log responses, it has been provisionally correlated with the Newmarket Till, which was deposited during the main phase of the Late Wisconsin ice advance (ca. 25-18 Ka BP; Nissouri Stadial) (Karrow, 1984, Boyce et al., 1999; Boyce and Eyles, 2000). The uppermost surficial Halton Till is typically a silty to sand-silt diamict and was deposited during a final re-advance of ice out of the Ontario basin, about 12-13.5 Ka BP (Port Huron Stadial; Karrow, 1984). The Halton Till is separated from an underlying, more consolidated diamict unit by sands and gravels deposited during the Mackinaw Interstadial (MIS). The MIS deposits in HR include fluvial, deltaic and lacustrine sediments (Costello and Walker, 1972).

Meyer and Eyles (2007) investigated the infill stratigraphy of several buried valleys in Halton Hills using continuously cored boreholes. They identified six lithostratigraphic units including two regionally extensive diamict units that they correlated with the Halton and Newmarket tills.

Slomka (2011) used sedimentological methods, including AEA, to study the outcrop stratigraphy of the Limehouse quarry. A total of nine sedimentary facies types and six architectural elements were identified and grouped into major sedimentary units or 'element associations'. Her study concluded that the Limehouse Pit sediments were deposited within a braided-river and delta-front environments with paleoflow directions toward the south and southwest. Her results were integrated within a conceptual 3-D facies model, which provides a basis for comparison with GPR results in this study.

Brennan (2011) used borehole geophysics and core data to investigate the Quaternary stratigraphy of buried valleys to southwest of Georgetown, Ontario. Conductivity, magnetic susceptibility, sonic and gamma logs were collected at 16 wells and integrated with log suites from pre-existing wells and archival data to produce a detailed 3-dimensional subsurface model. Brennan identified nine lithostratigraphic units, of which four units were identified as existing and/or potential aquifers. In agreement with Slomka (2011), Brennan identified a high level of heterogeneity within the Quaternary stratigraphy, particularly the Mackinaw Interstadial deposits.

1.2.5 Study Objectives

In this study, GPR surveys and outcrop studies were conducted at the Limehouse quarry to characterize the 3-dimensional sedimentary architecture of glaciofluvial deposits. The sediments host a regional shallow aquifer that has potential as an artificial recharge site. The specific objectives of the thesis were to:

1) characterize the sedimentary facies using detailed multi-frequency, 3-D GPR surveys and sedimentologic logging of outcrops;

2) investigate the 3-dimensional geometry of the gravel deposits through architectural element analysis (AEA) of radar facies and reflection patterns, and;

3) develop a conceptual depositional model for the Limehouse Pit with reference to previously published geological data (Slomka, 2011).

1.3 METHODS

1.3.1 Ground-penetrating Radar

GPR is a non-invasive, near-surface (<50 m) geophysical technique that uses high frequency (10 MHz – 2 GHz) electromagnetic (EM) waves to detect and image electrical discontinuities in the shallow subsurface (Fig. 1.3). When these waves encounter boundaries where the electric and/or magnetic properties of the ground change, part of its energy will be reflected and part of it will be transmitted (Mellet, 1995). Dielectric permittivity (ε), magnetic permeability (μ) and electrical conductivity (σ) are the three properties of the material governing how electromagnetic energy will behave in a given medium (Neal, 2004). Dielectric permittivity is a measure of how readily a material can store an electrical charge and is measured in farads per metre. Magnetic permeability can be regarded as the magnetic equivalent of dielectric permittivity and is measured in henrys (H) per metre. Both magnetic permeability and dielectric permittivity are

Figure 1.3: Principle of ground-penetrating radar (GPR) method (modified from Neal, 2004). A. high frequency radar impulse is transmitted into the ground and reflected at subsurface boundaries with contrasting relative permittivity (ε_r). The arrival of the reflected impulse is recorded by at the ground surface by a receiving antenna and the two-way travel time (TWT) is used determine the depth to the boundary. B. Typical radargram showing direct arrivals associated with air and ground waves and primary reflection events. The two-way travel times are converted to depth using the radar wave velocity estimated from diffraction hyperbolas or using the normal move-out (NMO) of reflections recorded on multi-channel radar records.

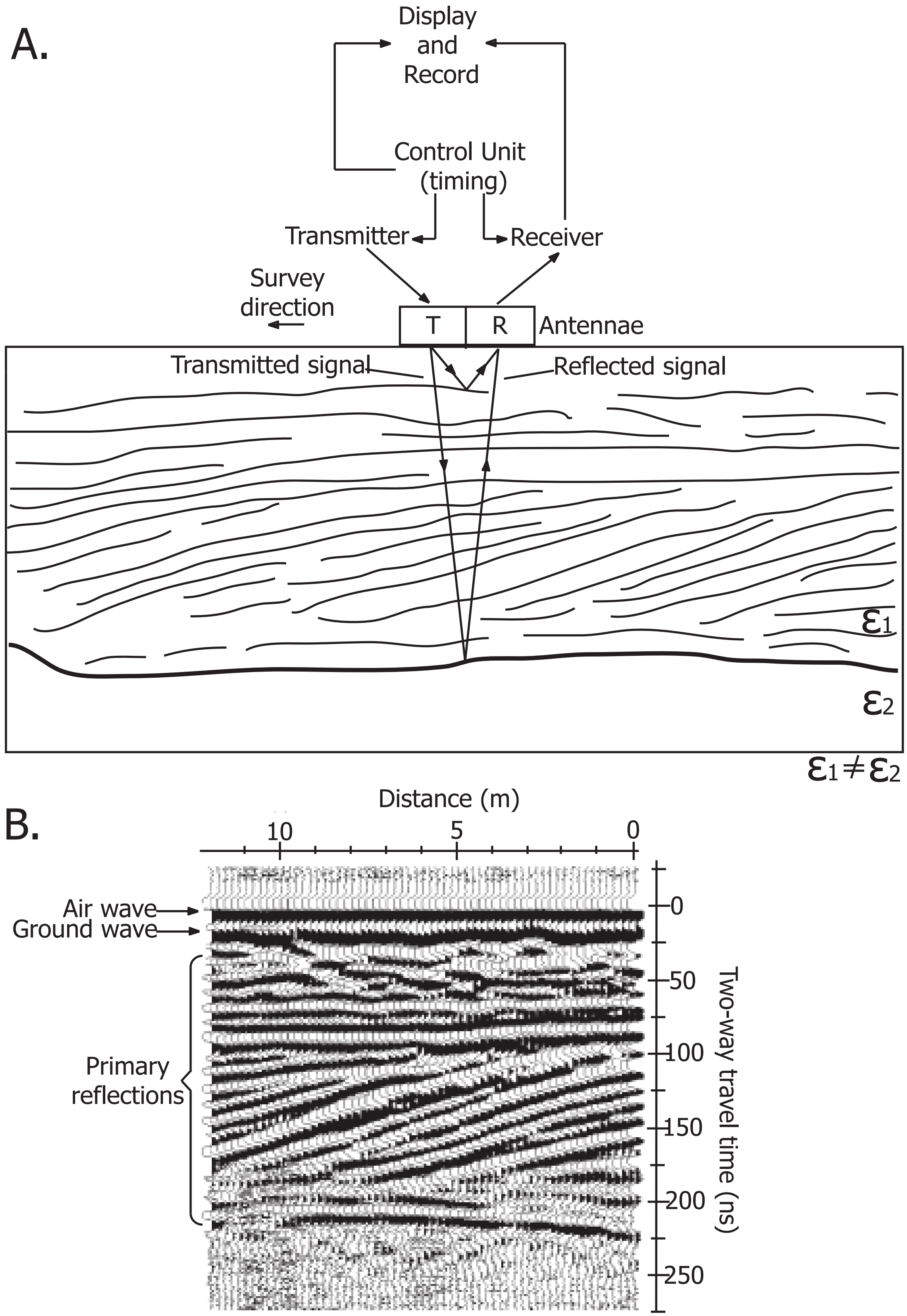
A.
Display
and
Record
Control Unit
(timing)
Transmitter
Receiver
Survey
direction
T
R
Antennae
Transmitted signal
Reflected signal
ε1
ε2
ε1≠ε2
B.
Distance (m)
10
5
0
Air wave
Ground wave
Primary
reflections
0
50
100
150
200
250
Two-way travel time (ns)

expressed relative to the permeability or permittivity of free space (an area containing no matter and no gravitational or electromagnetic fields). Conductivity measures the ease with which a charge can pass through a material once a static electric field is applied (Neal, 2004). The speed at which an electromagnetic wave moves through a medium is defined by the following equation:

$$v = \frac{c_0}{\sqrt{\varepsilon_r \mu_r \frac{1 + \sqrt{1 + (\sigma/\omega\varepsilon)^2}}{2}}}$$

(1)

where c_0 is equal to 3 x 10^8 m s^{-1} (the electromagnetic wave velocity in a vacuum), ε_r is the relative permittivity (dielectric constant), μ_r is the relative magnetic permeability, and $\sigma/\omega\varepsilon$ is a loss factor, where $\omega = 2\pi f$ is angular frequency, measured in rad s^{-1}(Neal, 2004). This equation can be simplified in low loss materials where the amount of loss from conductivity (σ) is nearly negligible. Under such conditions $\sigma/\omega\varepsilon \approx 0$ and propagation velocity is primarily controlled by medium's dielectric constant. For most geologic materials the value of the relative magnetic permeability, $\mu_r = 1$ and Equation (1) thus becomes:

$$v = \frac{c_0}{\sqrt{\varepsilon_r}}$$

(2)

Equation (2) shows that the dielectric permittivity of the material controls the velocity of the wave (Neal, 2004).

Furthermore, the amplitude of the electromagnetic wave passing through a medium declines at an exponential rate:

$$A = A_0 e^{-\alpha z} \tag{3}$$

where A is the amplitude, A_0 is the initial value of A, z is the distance traveled and α is the attenuation constant (Neal, 2004). The attenuation constant is defined by:

$$\alpha = \frac{\sigma}{2}\sqrt{\mu/\varepsilon} \tag{4}$$

Equation (4) shows that conductivity controls the attenuation (Neal, 2004).

When an electromagnetic wave is traveling through a medium and encounters a boundary where permittivity ε_r is contrasting, a portion of the energy is reflected. The strength of this reflection is equal to the magnitude of the contrast in relative permittivity and is measured by the reflection coefficient, R:

$$R = \frac{\sqrt{\varepsilon_{r2}} - \sqrt{\varepsilon_{r1}}}{\sqrt{\varepsilon_{r2}} + \sqrt{\varepsilon_{r1}}} \tag{5}$$

where σ and μ_r are assumed to be negligible and ε_{r1} and ε_{r2} are the relative dielectric permittivities of layers 1 and 2, which lie adjacent to one another (Neal, 2004). In equation 5 ε_{r1} and ε_{r2} can be replaced with v_1 and v_2 due to the fact that dielectric permittivity governs the velocity.

GPR can be used to define the types of sediment being encountered by the electromagnetic pulses emitted from the unit. The type of sediment can be interpreted from determining the speed at which the waves pass through the sediment. As expressed in equations (1) through (5), a clay or other highly conductive unit will cause the electromagnetic wave to be greatly attenuated. The lower the conductivity and saturation, the higher the amount of penetration that can be achieved by the GPR (Busby and Merritt, 1999). Therefore, GPR is excellent for use in sand and gravel areas like the Limehouse quarry, unless the sediments are highly chaotic or conductive materials (Neal, 2004). As the pulses penetrate deeper into the sediment the amount of detail in the shallower units diminishes, which means that it is necessary to carefully choose the penetration depth before beginning a survey (Davis and Annan, 1989). Once the survey is complete and the data is loaded into a processing program like RadExplorer, it is possible to create a velocity profile. Roughly four diffraction patterns are found within the radargram and a parabola is fit to each diffraction event, which measures the speed at which the pulse was travelling within the unit. In turn, each speed represents a type of sediment. For example, unconsolidated sand or gravel is present when the radio wave is travelling through the subsurface at roughly 5-12 cm/ns (Neal, 2004). Although this is not a conclusive means of determining subsurficial sediment types, it does give an idea.

Seismic reflection and refraction are often used in shallow subsurface geophysical studies, as they are not affected by clay or moisture content (Cardimona et al. 1998). Seismic methods, however, rarely provide the sub-metre scale vertical resolution that is required for most applied groundwater studies (Neal, 2004). Seismic surveys are also more costly and time consuming than GPR, which makes GPR a more realistic choice when time and money are of the essence (Cardimona et al. 1998). Not only are the techniques themselves different, but the images that these methods produce differ as well. In GPR:

i) the saturated and unsaturated zones are distinctly separated by the water table;

ii) there are an increased number of causes of signal scattering at or above the ground surface, e.g. cell phone waves can cause signal scattering;

iii) diffraction patterns are much more prevalent;

iv) the intended investigation depth is much shallower – typically less than 20 m;

v) there is extreme signal attenuation in conductive soils, such as clay, and;

vi) the wavelength emitted by the device is shorter (Van Overmeeren, 1998).

1.3.2 Data Acquisition

In this study, a multi-frequency GPR survey was conducted in the Limehouse gravel pit to investigate the subsurface architecture of thick glaciofluvial deposits. GPR data were acquired using four different frequencies (25, 50, 100 and 250 MHz). The 250 MHz data were acquired using a Sensors & Software Noggin 250 MHz radar system with a digital video logger (DVL) and Trimble Ag132 D-GPS (Fig. 1.4d and e). The 25, 50 and 100 MHz data were collected using a MALA RAMAC GPR with a ProEx Control Unit and external D-GPS (Fig. 1.4a, b, c, f and g). The MALA 25 and 50 MHz systems employed unshielded Rough Terrain Antennas (RTA) designed for use in areas with dense vegetation or rapidly changing topography (Fig. 1.4a-c). The 25 MHz antennas have a transmitter-receiver separation of 6.2 m and the 50 MHz a 4.8 m separation. The 100 and 250 MHz shielded antennas were more difficult to maneuver across the site due to their size but were less subject to radio interference.

Figure 1.4: Survey equipment used in the study. A. 25/50 MHz Mala rough terrain antenna (RTA) system, including video logger, control unit, carrying pack and D-GPS. B and C. RTA system in operation in quarry. D. 250 MHz sensors and software Noggin Plus GPR system with encoder wheel and Trimble D-GPS. E. 250 MHz unit in use. GPR and positioning data are recorded on the digital video logger (DVL). F. Mala 100 MHz shielded antenna showing encoding wheel, antenna and A/D converter. G 100 MHz antenna in use.


A
Carrying pack
Video logger
Control unit
Antenna
Timing mechanism
D
GPS
Encoding wheel
Antenna
B
GPS
E
C
F
A/D converter
Encoding wheel
Antenna
G

GPR profiles were acquired in three locations onsite (Fig. 1.2). Two radar survey ‘patches’ (Grid 1, 2; Fig. 1.5) were collected on the pit floor adjacent to the northeast wall of the Wilroy Pit. GPR profiles lines were laid out with 2 m separations in a NW-SE direction and at 20 m line spacings in the SW-NE orientation. String guidelines were laid out on the quarry floor and the survey equipment was pulled across the site by a two-person team (Fig. 1.4e and g). The GPR sounding positions were recorded in real time using D-GPS and the GPR survey wheel. Line positions and surface elevations were measured at 1 m intervals along the pit survey lines using a Magellan ProMark 3 D-GPS to improve the positional accuracy. Several 2-D profiles were also acquired on the roadway (4^{th} Line) adjacent to the pit and on top the 12-m high outcrop that forms the northeast pit wall (Fig. 1.2). The 250 MHz frequency was collected in the pit only, as it was determined from trial runs that there was limited penetration with this frequency along the roadway and outcrop due to the presence of the attenuating overlying sediment. In total, 53 profiles were collected using 250 MHz unit and 57 were collected with each of the 25, 50 and 100 MHz units, equaling 224 profiles.

Figure 1.5: GPR line layout for 3-D survey grids 1 and 2. Line spacing between x- and y-lines is 2 and 10 metres respectively.

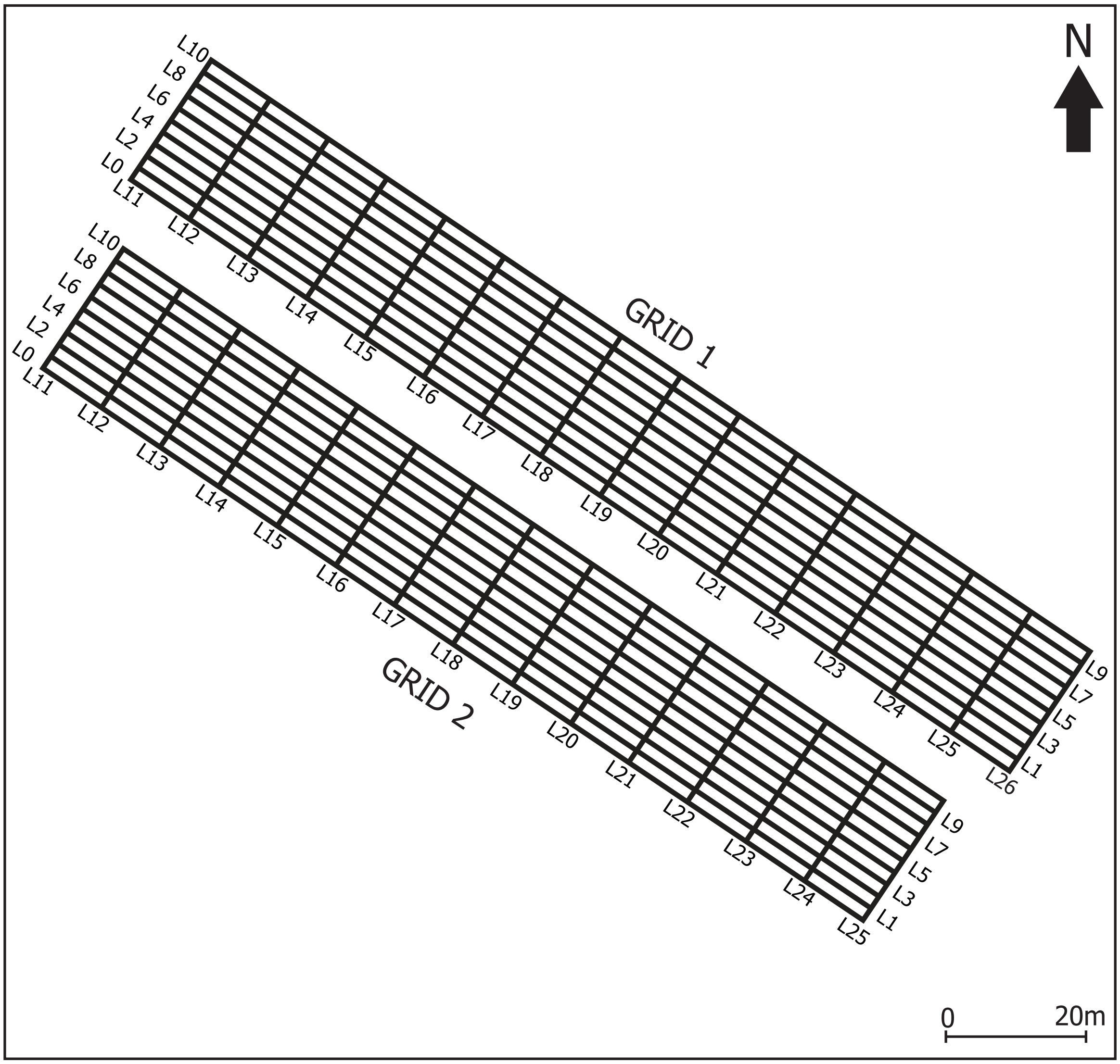
N
GRID 1
GRID 2
L10
L8
L6
L4
L2
L0
L11
L12
L13
L14
L15
L16
L17
L18
L19
L20
L21
L22
L23
L24
L25
L26
L9
L7
L5
L3
L1
0
20m

1.3.3 Data Processing

A suite of software was used to process the radar data including Oasis Montaj, RadExplorer, GPR-SLICE and SMT Kingdom Suite. Oasis Montaj was used to correct redundant or erroneous data points within both the GPS coordinate and topographic elevation data. Once completed, the radargrams were pulled into RadExplorer; a geophysical processing software produced by MALA Geosciences. The road and outcrop profiles were corrected only using this program as they were not needed in three-dimensional views, whereas the grids were further processed in GPR-Slice. The velocity profiles were completed on all grid profiles before any processing occurred. The processing steps for all datasets are (in order of completion): DC removal; time-zero adjustment (0 ns); background removal; amplitude correction (regain); bandpass filtering, and; topographic correction (Fig. 1.6).

GPR-SLICE is a ground penetrating radar imaging software used mainly for completing archaeological studies and it's delve into sedimentological and hydrogeological studies is relatively new with this project. GPR-SLICE was chosen for this study as it provides the user with a highly advanced means of quasi-3D volume creation from 2D datasets.

First a project is created and the data is imported. Once the import process is complete and the correct parameters of each dataset have been entered the program puts the data through a conversion step that adds a set amount of gain to the radargrams and removes the DC-drift (or 'wobble'). The user then performs a time-zero adjustment,

Figure 1.6: GPR data processing flow employed in GPR-SLICE software to produce 3-D radar volumes.

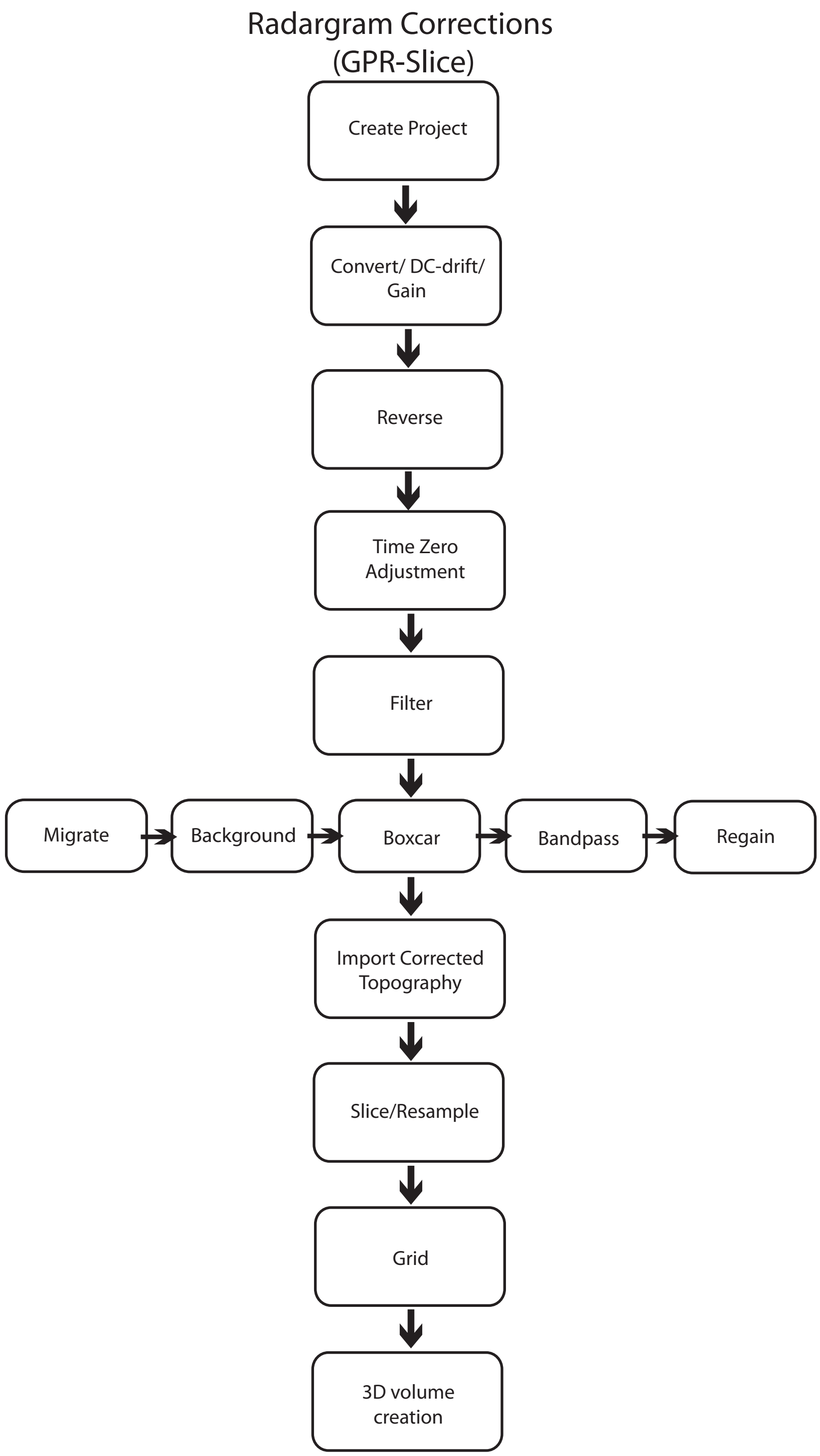
Radargram Corrections
(GPR-Slice)
Create Project
Convert/ DC-drift/ Gain
Reverse
Time Zero Adjustment
Filter
Migrate
Background
Boxcar
Bandpass
Regain
Import Corrected Topography
Slice/Resample
Grid
3D volume creation

which allows one to set the vertical scale to zero at the ground surface. After several other steps, the filtering process begins. Not all filtering steps were applied to every set of data and in some cases, such as the 100 MHz data where cell phone noise was present, more than one pass of some processing steps needed to be applied. In general, the flow processes and their importance are as follows:

1) Migration - Collapses hyperbolas to point reflections;

2) Background filter - Commonly used to remove banding noises seen across radargrams. It works by subtracting the average scan across a radargram from each individual trace within each profile. It is possible to remove strong linear reflectors while attempting to remove banding noises;

3) Boxcar Filter – Diminishes high-frequency random noise within radargrams. For the purposes of this study, the boxcar filter was used solely to 'widen' the cell phone noise present within the 100 MHz data from both grids one and two;

4) Bandpass filtering – Increases the signal to noise ratio. It filters amplitudes within a range chosen by the user. The high- and low-cutoff values are set within the spectra menu and the filter is applied. In the case of exterminating the cell phone noise, the high- and low-cutoff values were set to a very specific area and that frequency was removed;

5) Regain – Amplitude correction or Automatic Gain Control (AGC) is done by creating an appropriate gain curve and applying it to the data. Generally the gain curve takes on an exponential shape that increases with depth, as amplitudes in lower parts of the record typically need to be boosted more than those in shallower parts; and,

6) Topographic correction – Applies the corrected topography to the profiles.

Once all of the filtering was applied the profiles were sliced. The sliced files were then gridded and converted into quasi three-dimensional cubes. The x- and y- search radii were set so that the value in the x-direction was always smaller than in the y-direction. This was due to the fact that the data was collected with a larger distance between y-lines than x-lines and therefore less 'searching' for data had to be completed in the x-direction to find information. After the filtering and topographic corrections were applied to the profiles they were exported into Kingdom Suite for horizon picking.

1.3.4 Identifying AE's using GPR

Radar facies, radar surfaces and radar packages are used to define architectural elements within the GPR data. Radar surfaces are defined as bounding surfaces that define the top and bottom of radar facies and represent an erosional surface or other major bounding surface. Radar facies are the internal structure between these surfaces and are identified based on a number of reflection attributes, such as shape, dip and continuity. Radar packages are 3D, large scale external forms of the radar elements made up of both the radar surfaces and radar facies (Neal, 2004). Radar surfaces are indicated by amplitude changes, the relationship of the reflectors to one another and their geometry (e.g. cross-cutting). Using these attributes the order of the bounding surface can be identified. Table 1.1 defines how these bounding surfaces are described and classified.

From 0^{th} to 7^{th} order surfaces, the amplitude of each surface increases and becomes more prominent in the radargrams. The 250 MHz unit is best for defining 0^{th} – 4^{th} order surfaces, while the 50 MHz unit can better identify 5^{th} – 7^{th} order surfaces. 0^{th} order surfaces cannot be resolved with the 250 MHz unit, as their extent would fall below the 20cm resolution of the unit. 1^{st} order surfaces show a concordant top and bottom relationship with bounding radar facies. Facies on either side of the radar surface should be quite similar, as 1^{st} order surfaces separate like lithofacies. 2^{nd} order surfaces would also exhibit the concordant surface with their surrounding radar facies, but the facies atop and below the surface will be slightly different because 2^{nd} order surfaces define dissimilar lithofacies. 3^{rd} order surfaces are laterally discontinuous, so they would not have a large lateral extent. They are minor erosional surfaces so they could be disconcordant with their upper and lower radar facies. 4^{th} order surfaces are laterally continuous so they can be traced for 10's of metres within a radargram. They are associated with moderate-high amplitudes and can exhibit concordant and disconcordant relationships with their surrounding radar facies. 5^{th} order surfaces are laterally continuous, high amplitude reflectors that are able to be mapped out over 10's to 100's of metres. The lower boundary often shows baselap, while the upper boundary shows erosional truncation or toplap and they can significantly cross-cut lower order surfaces. 6th and 7th order surfaces are very high amplitude, largely continuous events that must be mapped out over a large-scale area. 6th order surfaces define stratigraphic units and would thus have a wide number of 5th order surfaces defining many architectural elements within them. 7th order units have several packages of stratigraphic units between them, each exhibiting their own architectural elements.

Table 1.1: Scheme used to describe and classify bounding surfaces in glacial strata from 0^{th} to 7^{th} order surfaces (Modified from Boyce and Eyles, 2000).

RANK	DEFINITION
0^{th} order	Laminae (e.g. shear laminations in Northern Till)
1^{st} order	Boundary separating like lithofacies within a lithosome
2^{nd} order	Boundary defining dissimilar lithofacies within a lithosome (e.g. minor sand/silt stringers in diamict element)
3^{rd} order	Minor erosion surface; laterally discontinuous
4^{th} order	Laterally continuous surface defining boundary between individual architectural elements (e.g. diamict elements in Northern Till)
5^{th} order	Laterally continuous erosion surface demarcating base of genetically-related architectural elements
6^{th} order	Surfaces marking boundaries of mappable stratigraphic units (e.g. top and base of Northern Till)
7^{th} order	Surfaces bounding major depositional systems in a basin fill complex (e.g., base of Pleistocene succession)

1.4 LAYOUT OF THESIS

This thesis is organized as a "sandwich thesis". This format can lead to some redundancy within the abstracts, introductions and conclusions of each chapter. Chapter 1 provides an overall introduction and background to the study and Chapter 3 summarizes the research conclusions. In Chapter 2, the infill stratigraphy of the Limehouse Pit is described utilizing radargrams, borehole geophysics and outcrop lithology and architectural element analysis is applied in order to create a three-dimensional subsurface model. Overall, the study identifies that the Limehouse Pit is comprised of alternating sand and gravel units, with trough-cross beds being the most common structure identified. It can also be inferred that the deposits were likely from a Gilbert-style delta. Chapter 3 summarizes the results and conclusions drawn from each individual chapter, discusses primary implications of the research set forth in this study and gives areas in which further work needs to be completed.

CHAPTER 2: ARCHITECTURAL ELEMENT ANALYSIS (AEA) OF GLACIOFLUVIAL DEPOSITS USING MULTI-FREQUENCY GROUND-PENETRATING RADAR (GPR)

ABSTRACT

The sedimentary architecture of a coarse-grained glaciofluvial deposit was investigated in a gravel pit near Limehouse, Ontario using multi-frequency ground-penetrating radar (GPR). The gravel pit is one of several sites being considered for artificial groundwater recharge. GPR surveys were acquired using four different frequencies (25, 50, 100 and 250 MHz) over a 5800 m^2 area of the gravel pit floor and along an adjacent outcrop and roadways. Pit profiles were acquired at 2 m line spacing using D-GPS positioning and processed to a quasi-3D volume. Radar reflection patterns were grouped into radar facies and interpreted using architectural element analysis (AEA) with reference to well-exposed outcrops (> 10 m) and a nearby geophysically logged borehole.

Five distinctive architectural elements were identified in radargrams and their geometries mapped over the pit base. Gravel bar (GB) and gravel foreset (GF) elements are packages of moderate to steeply-dipping (30-45°) inclined reflectors, recording the accretion of longitudinal gravel bars in a braided river and progradation of small Gilbert-type deltas. Gravel clinoform (GC) elements are large-scale (10-100's m length), low-angle (< 15°) sheet-like packages of reflectors, produced by delta front progradation. Vertical aggradation (VA) elements are sheet-like packages of horizontal reflectors

produced by the aggradation of outwash deposits on a low topography outwash plain. Channel (CH) elements define trough-like packages of reflectors produced by incision and down-cutting of spillway channels into pre-existing glaciofluvial deposits. Stacked successions of architectural elements defined two, large-scale radar packages (RP-1, RP-2) recording two distinct depositional phases. RP-1 (elements GC, CH, GB) records the progradation of a sub-aqueous fan delta into a shallow proglacial lake with paleoflows towards the southeast. RP-2 records a subsequent phase of incision of deltaic deposits by glaciofluvial spillways and infilling of channels by aggradation of braided river sand and gravel deposits.

Comparison of the radar profiles with borehole and outcrop data indicates that lithosome bounding surfaces are associated with changes in sediment texture and porosity. Lithosomes defined using radar reflection patterns can therefore be used to predict changes in sediment grain size and associated hydrogeologic parameters (e.g. hydraulic conductivity). For example, spatial trends in hydraulic conductivity in the Limehouse deposit are likely to be strongly controlled by coarse gravel-filled channel elements (CH), and can be predicted from their spatial distribution and subsurface geometry. These results demonstrate that multi-frequency GPR is a viable approach for evaluating spatial trends in sedimentary heterogeneity and can be applied at other sites under consideration for artificial recharge projects.

2.1 INTRODUCTION

Quaternary glacial sediments are the predominant surficial deposits across a large area of Canada and the northern United States and are of great economic importance as sources of aggregate (sand, gravel) and groundwater resources (Stephenson et al., 1988). In southern Ontario, Canada, rapid urban development around the Greater Toronto Area (GTA; current population > 6 million) is placing increasing demands on groundwater resources. These demands are most acute in outlying communities that are dependent on groundwater from private or municipal wells for drinking water and domestic uses.

In Halton Hills (towns of Georgetown and Acton), located in Halton Region (Fig. 2.1b), more than 40,000 residents are reliant on groundwater and the demand is expected to increase dramatically as the population grows to >90,000 by 2031 (Aquaresource, 2008). Due to a shortfall in water supply, a moratorium was placed on new residential development until new groundwater resources could be located. The shortfall could be met by water piped from Lake Ontario, but this option is costly and will not meet the growing demand for groundwater in outlying rural areas. In response to the shortfall, Halton Region (HR) initiated a systematic investigation in 2008 of the Quaternary geology and hydrostratigraphy of Halton Hills in collaboration with McMaster University (Brennan, 2011; Puckering, 2011; Slomka, 2011). A key objective of that study was to develop a better understanding of the subsurface stratigraphy and sedimentology of Quaternary deposits, which are the primary target for groundwater exploration. Previous work in HR had identified thick, high permeability sands and gravels within the

Figure 2.1: A. Surficial geology of southern Ontario showing locations of study site and Niagara Escarpment. B. Interpreted buried bedrock channels, and glaciofluvial spillway systems with paleoflow directions (modified from Slomka, 2011). C. Laurentide Ice Sheet (LIS) during its maximum extent over southern Ontario (ca. 22-16 Ka BP). D. Formation of Oak Ridges interlobate moraine between the Simcoe and Ontario lobes during LIS retreat (ca. 13 Ka BP) (modified from Slomka, 2011).

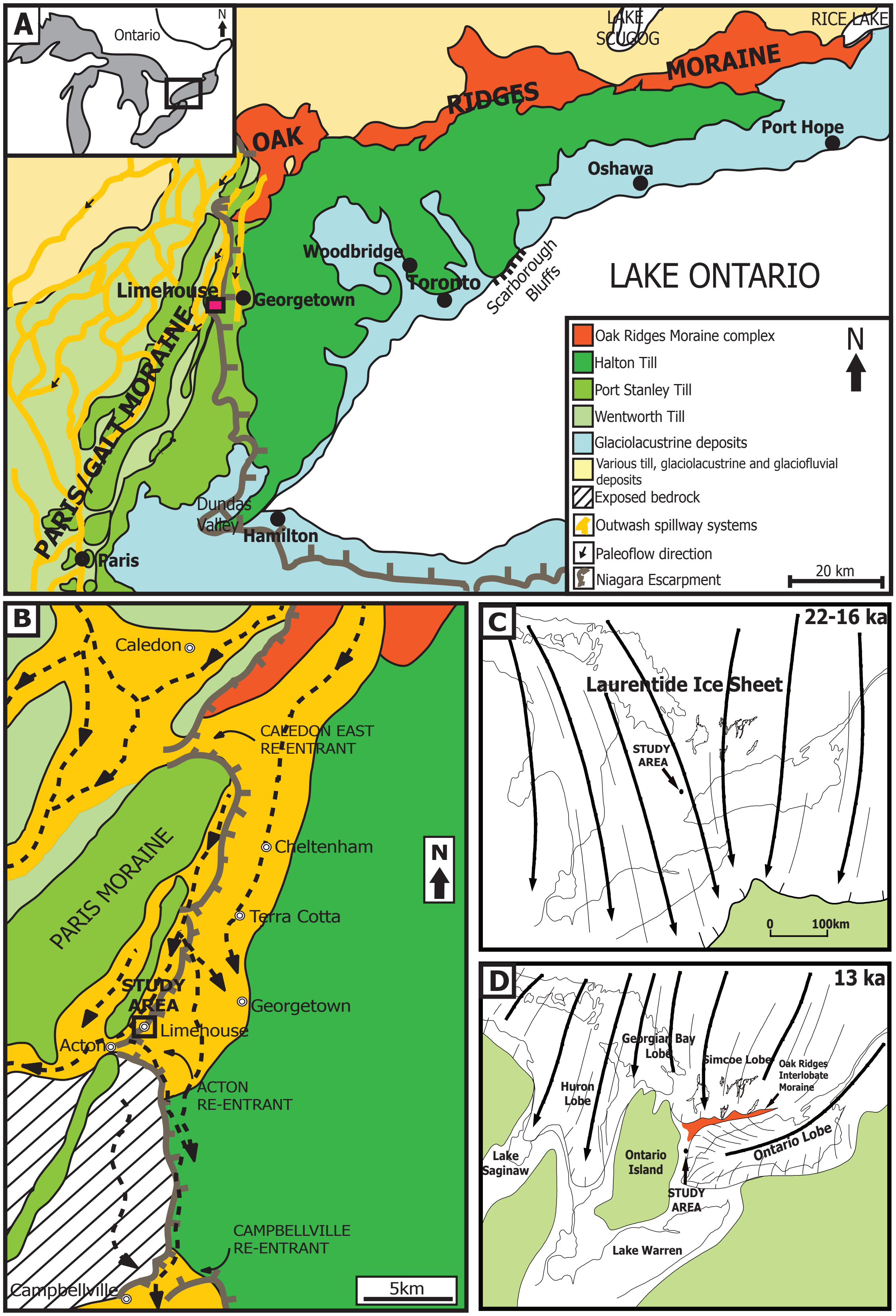
A
Ontario
N
LAKE SCUGOG
RICE LAKE
OAK
RIDGES
MORAINE
Port Hope
Oshawa
Woodbridge
Toronto
Scarborough Bluffs
LAKE ONTARIO
Limehouse
Georgetown
PARIS/GALT MORAINE
Dundas Valley
Hamilton
Paris
Oak Ridges Moraine complex
Halton Till
Port Stanley Till
Wentworth Till
Glaciolacustrine deposits
Various till, glaciolacustrine and glaciofluvial deposits
Exposed bedrock
Outwash spillway systems
Paleoflow direction
Niagara Escarpment
20 km
B
Caledon
CALEDON EAST RE-ENTRANT
Cheltenham
PARIS MORAINE
Terra Cotta
STUDY AREA
Georgetown
Limehouse
Acton
ACTON RE-ENTRANT
CAMPBELLVILLE RE-ENTRANT
Campbellville
5km
C
22-16 ka
Laurentide Ice Sheet
STUDY AREA
0 100km
D
13 ka
Georgian Bay Lobe
Simcoe Lobe
Oak Ridges Interlobate Moraine
Huron Lobe
Lake Saginaw
Ontario Island
STUDY AREA
Ontario Lobe
Lake Warren

Quaternary deposits with potential to supply high yield wells (Meyer and Eyles, 2007). These deposits are hosted within broad buried bedrock valleys but the location and extent of the valley systems and the Quaternary hydrostratigraphy needed to be better resolved in order to understand the groundwater resource availability (Brennan, 2011; Puckering, 2011; Slomka, 2011).

Due to the current groundwater shortfall HR is also investigating the feasibility of artificial recharge of regional aquifers using surface waters. Artificial recharge is the replenishment of groundwater by the infiltration or pumping of water into surface recharge aquifers. Typically, sites are selected where the surficial sediments are highly permeable, allowing surface waters to rapidly recharge into underlying aquifers. In cases where high permeability surficial sediments are not present, water can be injected into aquifers through wells or trenches excavated into the unsaturated zone (Freeze and Cherry, 1979). The water for artificial recharge can come from streams regulated with dams, storm runoff, aqueducts and water treatment plants (both drinking water and sewage).

A number of potential groundwater recharge areas have been identified in Halton Hills where the surface sediment type and hydrostratigraphy are favourable for an artificial recharge project. These include areas where coarse-grained glaciofluvial deposits are exposed at the surface (Fig. 2.1b) and are in direct hydraulic communication with underlying regional aquifers. Brennan (2011) identified a number of locations in the Georgetown area where shallow aquifers hosted in interstadial sand and gravel deposits

(Mackinaw Interstadial sediments, (MIS) are in direct communication with deeper aquifers. The MIS are characterized by a high level of sedimentary heterogeneity and vary significantly in thickness and lateral extent across southern Ontario (Boyce et al., 1995; Gerber and Howard, 2002). The evaluation of the groundwater resource potential and artificial recharge capacity of the MIS requires a detailed understanding of their sedimentary characteristics; in particular, their 3-dimensional geometry and textural variability, as these factors strongly control groundwater movement in glaciofluvial deposits (Anderson, 1989; Beres et al., 1999; Oldenborger et al., 2003).

The study of glaciofluvial deposits and their hydrogeologic properties is increasingly aided through the use of near-surface geophysical methods, including ground-penetrating radar (GPR). A number of recent studies have shown that 2- and 3-dimensional GPR surveys are effective for studying the internal architecture or 'geometry' of complex sand and gravel deposits over a variety of length-scales (Huggenberger, Meier and Pugin, 1994; Olsen and Andreasen, 1995; Asprion and Aigner, 1997; Van Overmeeren, 1998; Asprion and Aigner, 1999; Beres et al. 1999; Bersezio et al., 2007; Kostic and Aigner, 2007; Goutaland et al. 2008). GPR methods employing radar impulses in the 25 MHz to 1 GHz frequency range are typically capable of resolving sedimentary layering with a vertical resolution of decimeters to metres at depths of investigation up to 40-50 m (Neal, 2004). Detailed images of the internal bedding structure of sedimentary deposits can be employed to map the deposit geometry using radar facies and architectural element analysis (AEA). A number of studies have demonstrated the successful application of AEA methods to the interpretation of GPR data in hydrogeological and sedimentological studies. Stephens (1994) mapped the bedding structure of Lower Jurassic sandstones and compared the architectural elements derived from outcrop mapping. Asprion and Aigner (1997, 1999) examined the radar reflection patterns in Quaternary glaciofluvial deposits and Triassic fluvial sandstones in Germany and used them to classify architectural elements and identify hydraulic flow units. They advocated the use of GPR as a tool for studying outcrop analogues for subsurface aquifers and for developing hydrofacies models. Beres et al., (1995, 1999) employed 2-D and 3-D radar facies analysis and architectural elements to define heterogeneity trends and groundwater paths in Rhine Valley glaciofluvial aquifers. Szerbiak et al. (2001) characterized the heterogeneity in the Ferron sandstone using 3-D GPR and employed the radar amplitude data to generate a geostatistical model of the reservoir permeability. Bersezio et al. (2007) mapped fluvial architectural elements in Quaternary alluvial sediments using GPR integrated with surface resistivity measurements. Goutaland et al. (2008) employed radar facies to identify sedimentary architecture of glaciofluvial deposits underlying and infiltration basin. Bayer et al. (2011) combined 3-D GPR and outcrop measurements of sediment permeability to map the hydraulic conductivity trends in glaciofluvial aquifers in southern Germany.

In this study, we employed multi-frequency ground-penetrating radar (GPR) and architectural element analysis (AEA) of radar facies to characterize the sedimentary heterogeneity of thick (> 30 m) glaciofluvial sand and gravel deposits exposed in a quarry near Limehouse, Ontario (Fig. 2.2). The site is one of several open pit quarries currently actively mined for aggregates and crushed stone in the Halton Hills area (Fig. 2.1b).

Figure 2.2: Aerial photo of Wilroy and Duff-Bott pits showing location of 3-D GPR survey Grids (1 and 2) and 2-D radar profiles. The pit stratigraphy is well exposed in a 12 m high outcrop located on the northeast wall of the pit. Location of MW-22 monitoring well also shown.

58016879, 4832152.12 580543.43, 4832144.15

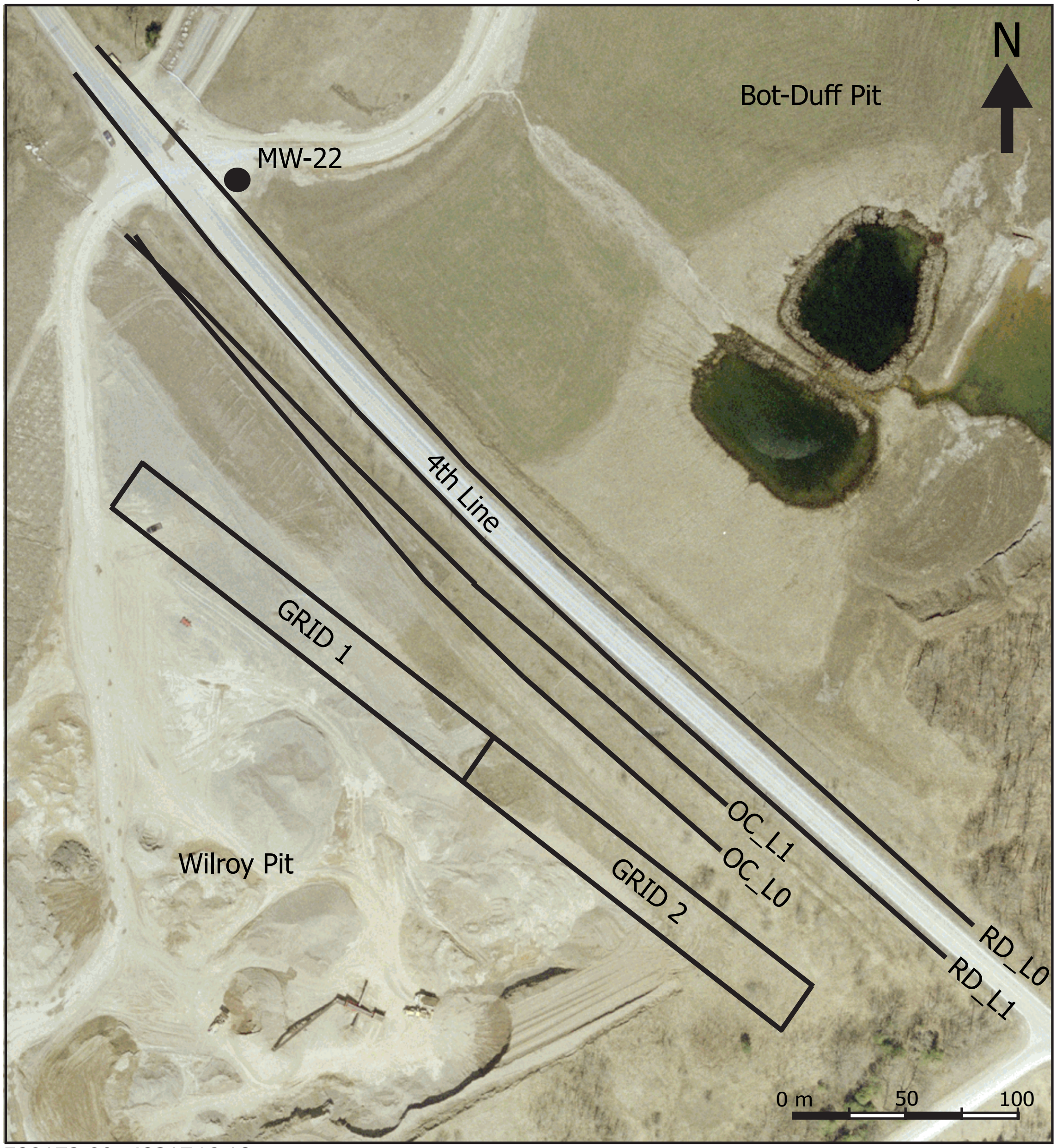

580172.09, 4831746.18 580542.08, 4831748.95

Once decommissioned, the quarries could serve as potential sites for artificial recharge of an underlying bedrock aquifer (Amabel Formation). The glaciofluvial deposits are well exposed in a 12-metre outcrop, allowing direct comparison of outcrop lithofacies with GPR profiles and 3-D volume slices. The sedimentary facies and architecture of the sand and gravel deposits were studied in detail by Slomka (2011) and summarized in a conceptual depositional model. The GPR data acquired in this study provide additional details of the 3-dimensional subsurface geometry of the deposit and give baseline information for modeling of the groundwater flow and recharge capacity. The GPR and outcrop data from the Limehouse quarry provide an important analogue for understanding the sedimentary characteristics and geometry of other coarse-grained glaciofluvial deposits present in the subsurface below southern Ontario and in other glaciated terrains in North America and Europe.

2.2 STUDY AREA

2.2.1 Site Location and Geology

The study site is a 62 Ha sand and gravel quarry located near the town of Limehouse, Ontario (Fig. 2.1b). The quarry has two active pits: the Bot Duff pit, located between 4th and 5th Lines and north of Sideroad 22, and the Wilroy Pit located to the west of 4th line, north of Glen Lawson Road (Fig. 2.2). GPR surveys were conducted on the floor of the Wilroy pit and along the east wall of the quarry adjacent to the 4th Line (Fig. 2.2). Prior to GPR survey work, the eastern face of the pit had been excavated during mining operations, exposing glaciofluvial sand and gravel deposits in a 10-12 m high outcrop. The glaciofluvial sediments host a shallow aquifer that functions locally as a recharge area where it is exposed at surface (Holysh, 1985; Brennan, 2011).

The surficial geology of the Halton Hills was mapped previously by Karrow (1963, 1984) who identified two regionally extensive tills sheets (Halton and Wentworth Tills) separated by poorly-sorted glaciofluvial (Mackinaw Interstadial) sand and gravel deposits (Barnett, 1991, Boyce et al., 1995). The lowermost till is typically a sandy, heavily consolidated diamict, deposited during the main phase of Late Wisconsin ice advance (Nissouri Stadial; ca. 25-18 Ka BP). The till is stratigraphically equivalent to the Newmarket Till recognized in the eastern GTA (Barnett, 1991; Boyce and Eyles, 2000) and is present in the subsurface across a large area of Halton Region (Meyer and Eyles, 2007). The uppermost surficial Halton Till was deposited during a final re-advance of ice out of the Ontario basin at about 13 Ka BP. The Mackinaw Interstadial (MIS) sediments separating the two tills were deposited during a brief ice-free period in southern Ontario between 14-13.2 Ka BP (Karrow, 1984; Boyce et al., 1995; Meyer and Eyles, 2007). The MIS sediments consist chiefly of poorly-sorted sands and gravels and more limited fine-grained silt and clays deposited in wide range of proglacial environments (e.g. outwash plains, sub-aqueous fan-deltas, lakes) (Costello and Walker, 1972; Slomka, 2011).

Quaternary deposits in Halton Hills reach a maximum thickness of 75 m within a system of broad bedrock valleys to the east of the Niagara Escarpment (Fig. 2.1b) (Meyer and Eyles, 2007; Brennan, 2011). The bedrock consists of Ordovician shales in the lowland areas to the east of the Niagara Escarpment and more resistant limestones and dolostones along the Escarpment. Core data from test well MW-22, located on 4th Line, indicates 26 m of Quaternary deposits overlying limestone bedrock (Guelph-Amabel Formation) (Lymburner, 2010; Brennan, 2011). The stratigraphy includes an uppermost succession of sand and gravel overlying a >10 m thick sandy diamict and lowermost sand and gravel unit on limestone bedrock. The diamict unit is not evident in the outcrop or in the subsurface below the Wilroy Pit, due to non-deposition or erosion. The glaciofluvial sediments exposed in the east face of the Wilroy Pit are capped by a thin, reddish sandy to silty diamict that is interpreted as Halton Till (Lymburner, 2010). The age of the underlying glaciofluvial sediments is not yet known, but based on their stratigraphic position they are assigned provisionally in this study to the Mackinaw Interstadial.

2.3 METHODOLOGY

2.3.1 Ground-penetrating Radar

GPR data were acquired across a 5800 m^2 area of the Wilroy Pit (Fig. 2.2) using four different frequencies (25, 50, 100 and 250 MHz) (Fig. 2.3). The 25, 50 and 100 MHz data were collected using a MALA ProEx (Fig. 2.3a-c and f-g) and the 250 MHz data using Sensors & Software Noggin 250 (Fig. 2.3 d-e). The 25 and 50 MHz systems employed MALA Rough Terrain Antennas (RTA), consisting of a transmitter/receiver array housed in a flexible tow cable for rapid surveying of uneven topography. The 100 and 250 MHz data were acquired using conventional shielded antennas. Survey positioning was recorded using a Trimble Ag132 differential GPS (D-GPS) and a wheel odometer system attached to the shielded antennas. The survey navigation was aided by placement of marker strings between survey line end points. As a further quality control step, the line positions and surface elevations were measured at 1 m intervals along all survey lines using a ProMark3 D-GPS with sub-centimetre positional accuracy. The high quality D-GPS elevation data were used to produce a digital elevation model for topographic correction of radar profiles (Neal, 2004).

The 3-D survey area was subdivided into two separate grids with dimensions 150 metres by 20 metres (Grid 1) and 140 metres by 20 metres (Grid 2) (Figs. 2.2, 2.4). The survey lines were spaced 2 metres apart with perpendicular tie lines at 10-metre spacing (Fig. 2.4). The inline sampling rate varied depending on the antenna frequency from 0.25 cm sampling for the 25 MHz profiles to 0.5 cm spacing for the 250 MHz surveys.

2-D radar profiles were acquired atop the 12 m high outcrop on the east wall of the Wilroy Pit and adjacent to the roadway on 4th Line (Fig. 2.2). The outcrop profiles were acquired using the 25, 50 and 100 MHz data for the purpose of comparison of the radar facies with outcrop photographs and lithofacies logs.

Fig. 2.3: Survey equipment used in the study. A. 25/50 MHz Mala rough terrain antenna (RTA) system, including video logger, control unit, carrying pack and D-GPS. B and C. RTA system in operation in quarry. D. 250 MHz sensors and software Noggin Plus GPR system with encoder wheel and Trimble D-GPS. E. 250 MHz unit in use. GPR and positioning data are recorded on the digital video logger (DVL). F. Mala 100 MHz shielded antenna showing encoding wheel, antenna and A/D converter. G 100 MHz antenna in use.


A
Carrying pack
Video logger
Control unit
Antenna
Timing mechanism
D
GPS
Encoding wheel
Antenna
B
GPS
E
C
F
A/D converter
Encoding wheel
Antenna
G

Figure 2.4: GPR survey layout. Survey was acquired in two separate 3-D grids. Line spacing between x- and y-lines is 2 and 10 metres respectively.

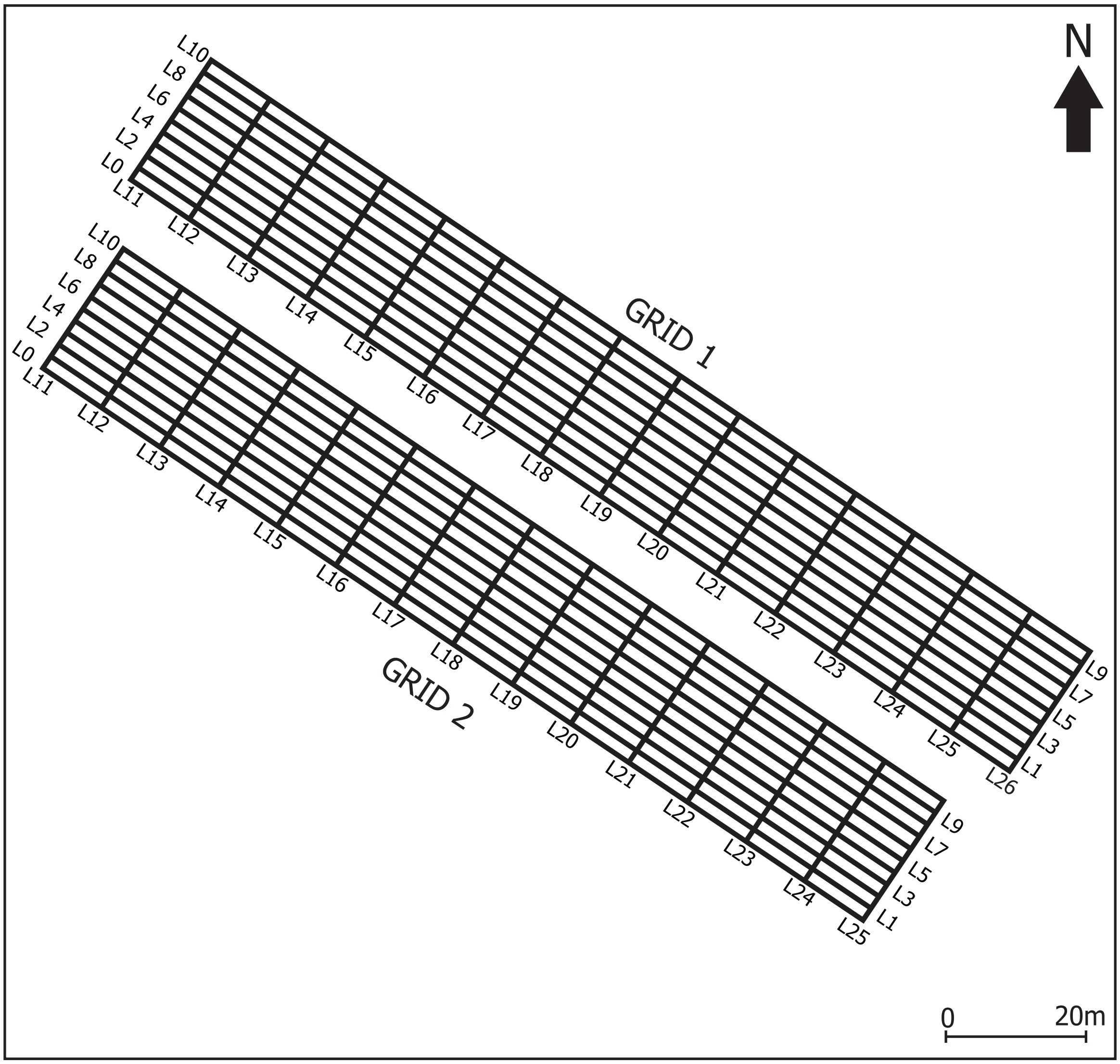
N
GRID 1
GRID 2
L0
L2
L4
L6
L8
L10
L11
L12
L13
L14
L15
L16
L17
L18
L19
L20
L21
L22
L23
L24
L25
L26
L1
L3
L5
L7
L9
0
20m

2.3.2 GPR Processing

The 2-D GPR profiles were processed in RadExplorer™ using a conventional radar processing flow as outlined by Neal (2004). The processing flow included import and editing of bad traces, zero-time adjustment, application of background (dewow) and band-pass filters, automatic gain control and topographic corrections. The profiles were then migrated using the Kirchhoff method and depth-converted using the average radar velocity obtained from curve fitting of diffraction hyperbolas. The 3-D survey data were processed in GPR-SLICE™, a software package designed for radar volume processing and interpretation. The GPR-SLICE™ processing flow (Fig. 2.5) employed the same steps as the 2-D data to produce fully corrected and migrated 2-D radar profiles. The 2-D data were then sliced and resampled at a 1 ns interval and gridded to a quasi-3-D radar volume using an inverse distance algorithm and 0.05-0.1 m grid cells. The completed 3-D radar volumes for each frequency are shown in Figure 2.6.

Figure 2.5: GPR data processing flow employed in GPR-SLICE software.

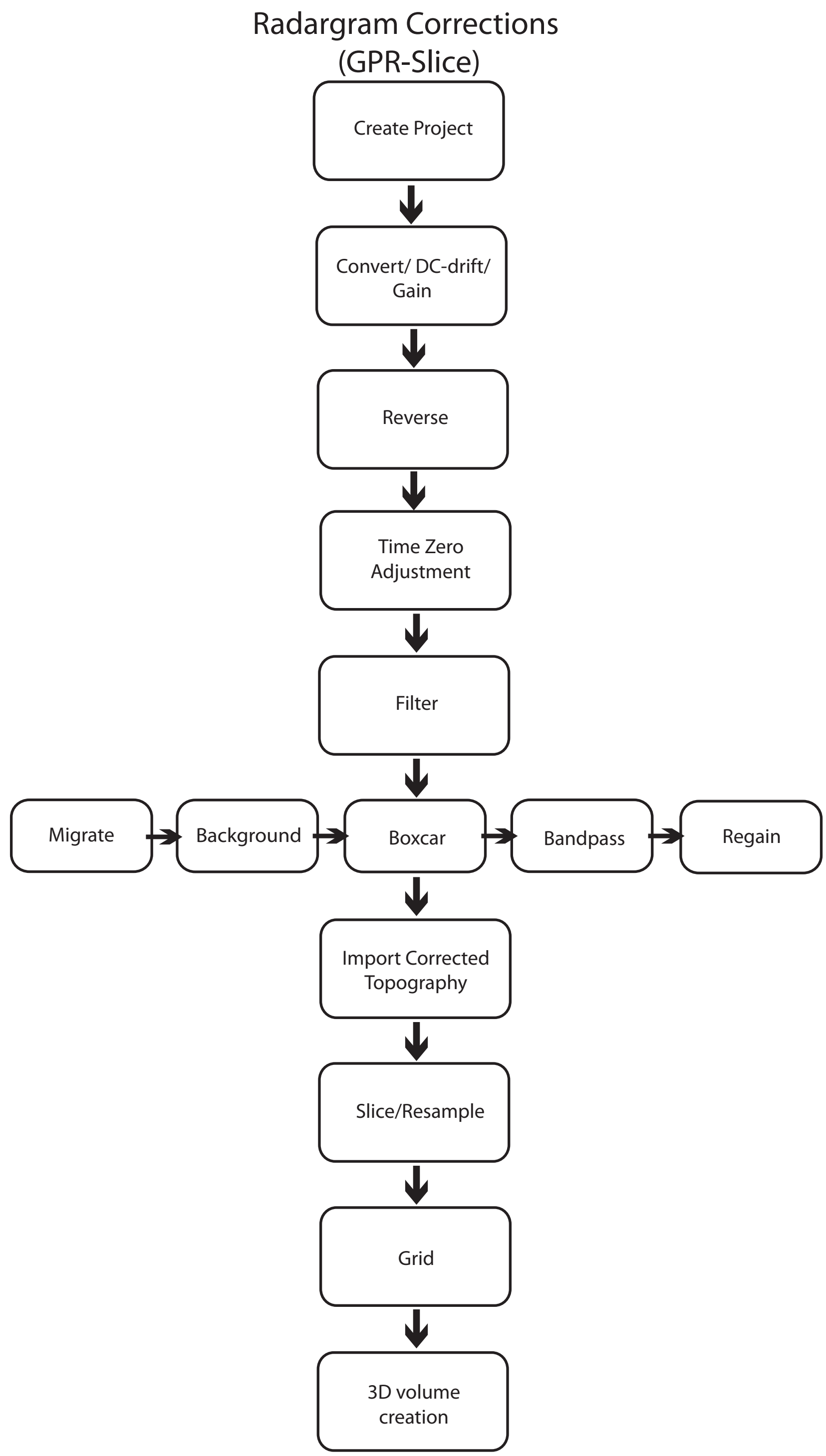
Radargram Corrections
(GPR-Slice)
Create Project
Convert/ DC-drift/
Gain
Reverse
Time Zero
Adjustment
Filter
Migrate
Background
Boxcar
Bandpass
Regain
Import Corrected
Topography
Slice/Resample
Grid
3D volume
creation

Figure 2.6: 3-D GPR volumes created in GPR-SLICE by interpolation of 2-D profiles (Grid 2). Data were gridded with 0.1 m cells using an inverse-distance algorithm. Note increase in vertical resolution and decrease in penetration depth with increasing frequency. Low frequency 25 and 50 MHz (A. and B, respectively) data resolve major bounding erosional surfaces (5^{th}, 6^{th} order) defining the base of channels and cross-cutting of lower order surfaces. The 100 and 250 MHz data (C. and D., respectively) resolve lower order surfaces, including 4^{th} order bounding surfaces that define individual lithosomes. Note large west-east oriented channel truncating southwestward dipping gravel clinoforms.

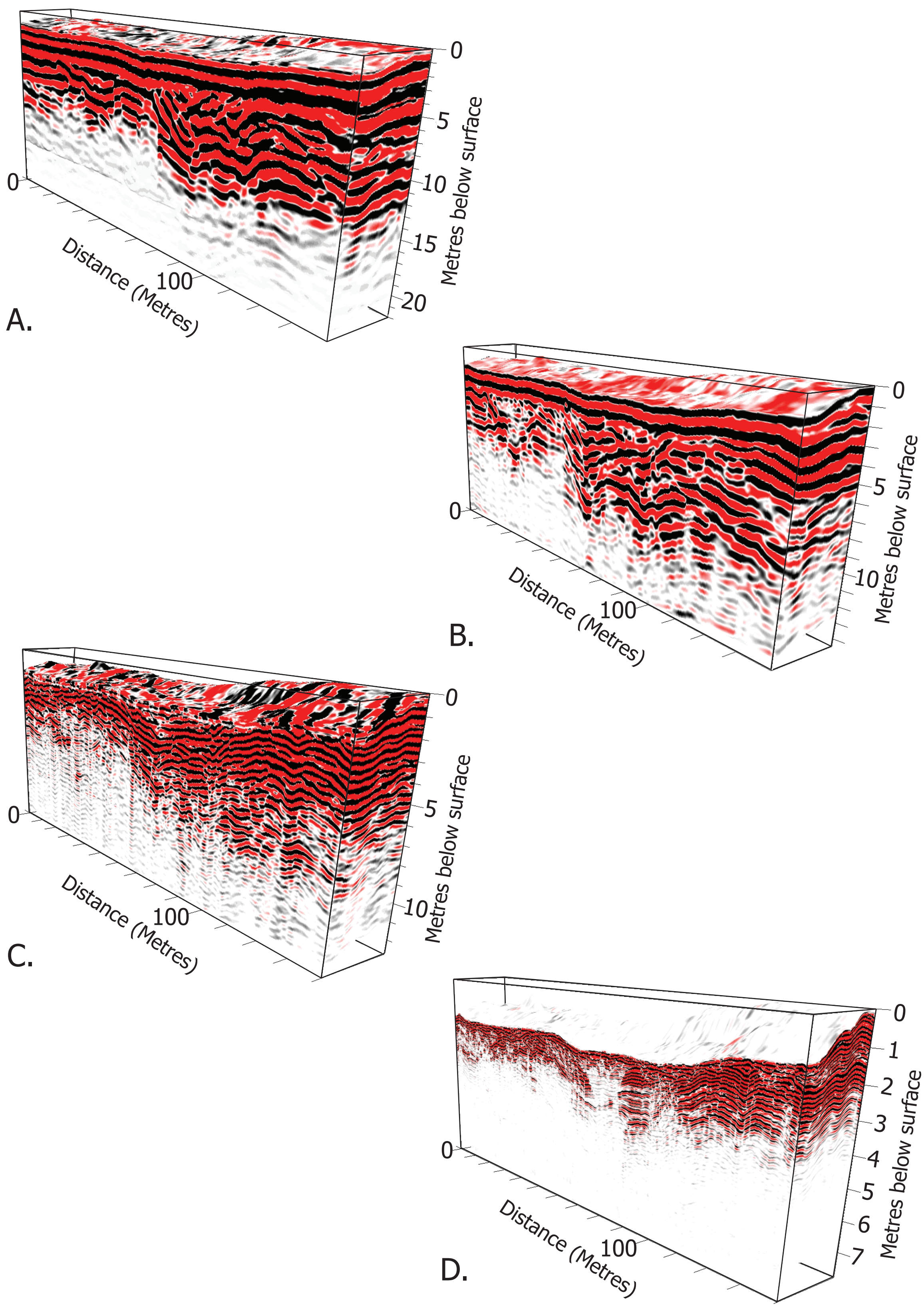

A.
0
Distance (Metres)
100
0
5
10
15
20
Metres below surface
B.
0
Distance (Metres)
100
0
5
10
Metres below surface
C.
0
Distance (Metres)
100
0
5
10
Metres below surface
D.
0
Distance (Metres)
100
0
1
2
3
4
5
6
7
Metres below surface

2.3.3 GPR Interpretation

The interpretation of 2-D profiles and 3-D radar volumes followed the scheme of Neal (2004), with the aim of keeping descriptive and interpretive terms separate. Neal (2004) proposed three fundamental building blocks to describe radar stratigraphy: radar surfaces, radar facies and radar packages (Fig. 2.7). Radar surfaces are defined as major bounding surfaces that define the top and bottom of a radar facies. In most cases they are analogous to sequence boundaries in seismic stratigraphy (Mitchum et al., 1977) and represent erosional surface or other major bounding surfaces separating genetically similar sedimentary facies. If the water table is present a high amplitude surface similar to a bounding surface can also be produced (Mitchum et al, 1977). Radar facies, which are bounded by radar surfaces, are identified based on a number of reflection attributes including reflector shape, dip, continuity and the relationship between reflections (Neal, 2004) (Fig. 2.7). Changes in the amplitude (relative reflection strength) and phase of reflection events can also provide additional useful attributes for radar facies discrimination. Radar packages are used to describe the external 3-dimensional form of radar facies. They are directly analogous to major bounding surfaces used to define architectural elements using the methods of Miall (1983).

As a final interpretive step, 2-D profiles and volume slices were imported to Kingdom Suite™ software for picking of reflection horizons and identification of radar facies and packages. The horizons were picked using amplitude changes, the geometry of the surface and also its relationship with other reflectors. Selected radar surfaces representing major bounding surfaces were then exported to Oasis Montaj^{TM} and gridded to produce 2.5-D surfaces for interpretation. The 2.5-D surfaces were employed along with radar facies to identify architectural elements and to interpret the depositional processes.

Figure 2.7: Terminology used to define and describe radar surfaces, radar packages and radar facies (modified from Neal, 2004).

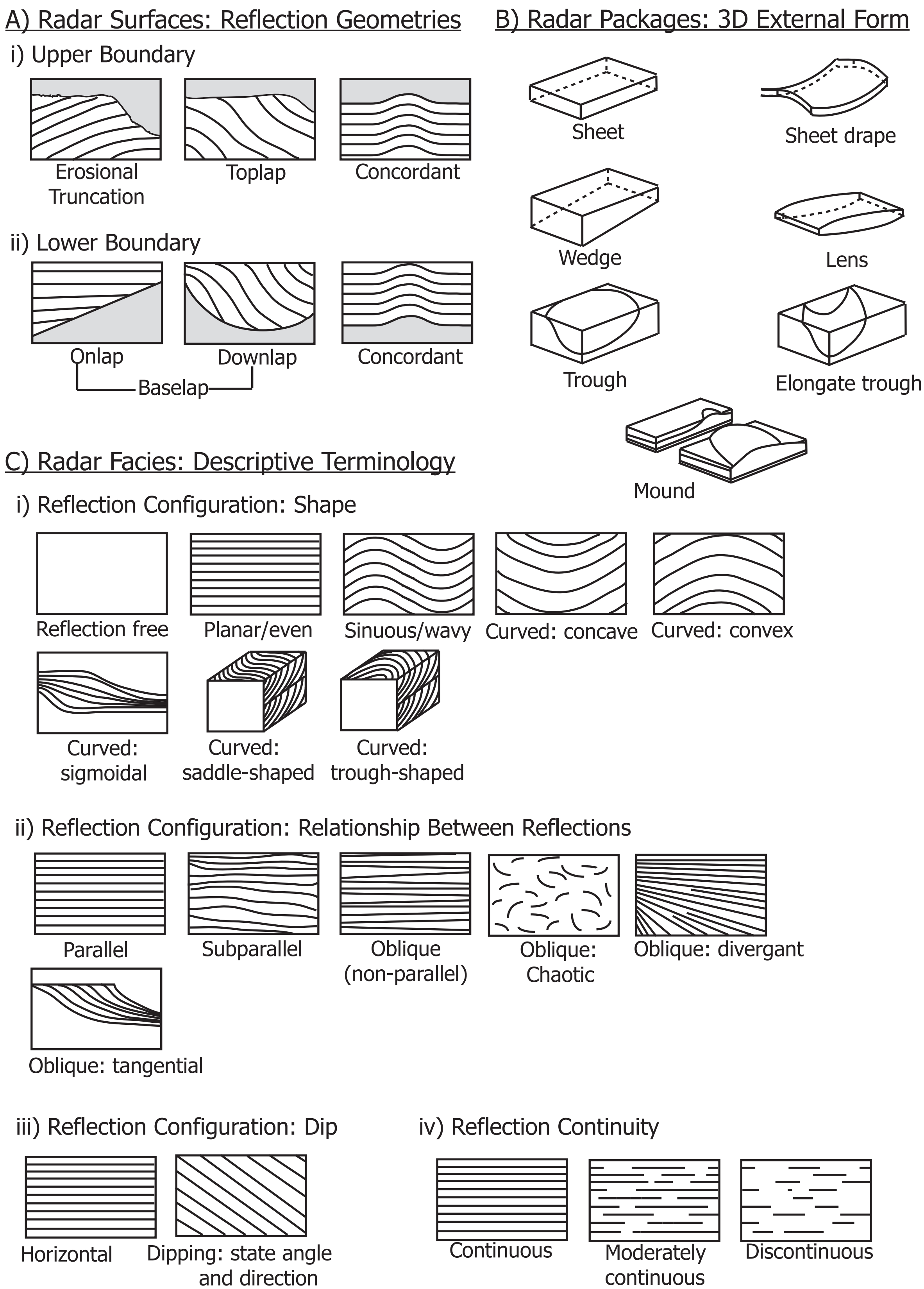
A) Radar Surfaces: Reflection Geometries
i) Upper Boundary
Erosional Truncation
Toplap
Concordant
ii) Lower Boundary
Onlap
Downlap
Concordant
Baselap
B) Radar Packages: 3D External Form
Sheet
Sheet drape
Wedge
Lens
Trough
Elongate trough
Mound
C) Radar Facies: Descriptive Terminology
i) Reflection Configuration: Shape
Reflection free
Planar/even
Sinuous/wavy
Curved: concave
Curved: convex
Curved: sigmoidal
Curved: saddle-shaped
Curved: trough-shaped
ii) Reflection Configuration: Relationship Between Reflections
Parallel
Subparallel
Oblique (non-parallel)
Oblique: Chaotic
Oblique: divergant
Oblique: tangential
iii) Reflection Configuration: Dip
Horizontal
Dipping: state angle and direction
iv) Reflection Continuity
Continuous
Moderately continuous
Discontinuous

2.3.4 Outcrop Studies

Lithostratigraphic logs were constructed at 6 locations on the outcrop (Fig. 2.8). At each location, the vertical succession of lithofacies was described in detail using the lithofacies codes of Eyles et al., (1983). Lithofacies were identified according to sediment texture (grain size), level of sorting, support mechanism, clast lithology and shape and sediment colour. Individual lithofacies were in turn grouped into five separate lithofacies assemblages, which are interpreted as genetically-related sedimentary facies deposited during a single phase of deposition (Units A-E, Fig. 2.8).

Lithofacies assemblages were compared with 2-D outcrop radar profiles and photomosaics in order interpret the radar facies in the 3-D subsurface data and to aid in identifying architectural elements and radar packages. Architectural element analysis (AEA) highlights the description of lithofacies assemblages and their geometry as defined by bounding discontinuities (Asprion and Aigner, 1999). Architectural element analysis allows for a hierarchical classification of bounding surfaces in both the vertical and lateral extent (Miall, 1985; Boyce and Eyles, 2000). In this study AEA was applied to both outcrop and GPR data to define the vertical and spatial extent of heterogeneities (e.g. the lateral extent and continuity of sands or gravels) within the Wilroy Pit.

Figure 2.8: Outcrop lithofacies logs for northeast wall of Wilroy Pit. Locations shown in inset. Lithofacies codes after Eyles et al. (1983). The major facies within the sand units are massive (Sm), current ripples (Sr), planar cross-bedding (Sp) and trough-cross bedding (St). The major facies within the gravel units are massive (Gm), planar tabular cross bedding (Gc) and stratification (Gs). Sandy diamict is represented by (Ds)

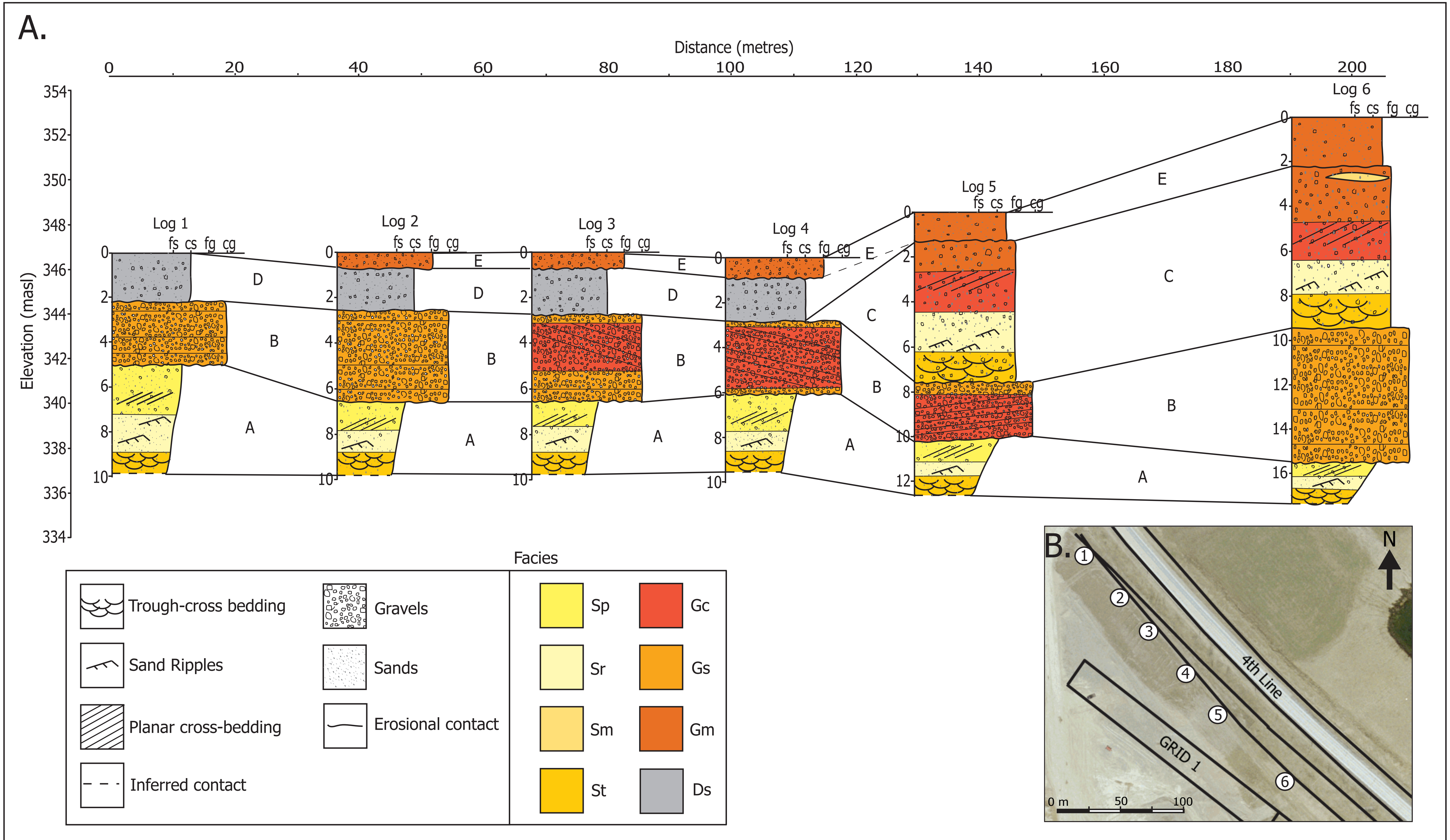

A.
Distance (metres)
0
20
40
60
80
100
120
140
160
180
200
Elevation (masl)
354
352
350
348
346
344
342
340
338
336
334
Log 1
Log 2
Log 3
Log 4
Log 5
Log 6
fs cs fg cg
A
B
C
D
E
Facies
Trough-cross bedding
Gravels
Sand Ripples
Sands
Planar cross-bedding
Erosional contact
Inferred contact
Sp
Gc
Sr
Gs
Sm
Gm
St
Ds
B.
N
1
2
3
4
5
6
4th Line
GRID 1
0 m
50
100

2.4 RESULTS

2.4.1 Lithofacies Assemblages

Five distinctive lithofacies assemblages were identified in outcrop (Units A–E, Fig. 2.8). Unit A comprises a thick package (> 2 m) of coarsening-upwards sandy facies at the base of the outcrop. Unit A and was subdivided into two sub-units based on texture (A_1, A_2). A_1 is a light beige, well-sorted fine to medium sand containing a variety of traction current bedforms, including current ripples, planar cross-bedding and trough-cross bedding (Sr, Sp, St). Unit A_2 erosively overlies A_1 and consists of dark brown, moderate to poorly-sorted coarse sand with gravel. A_2 contains both massive to crudely stratified sands (Sm) and planar cross- stratified sands with paleocurrents directed generally to the southeast to southwest.

Unit B is a thick (2-5.5 m) poorly-sorted gravel with pebbles and cobbles overlying Unit A across a sharply erosive contact (Fig. 2.8). The gravels are clast-supported with a poorly-sorted gravelly-sand matrix. The gravel body is sub-divided into a number of stacked, crudely stratified (Gs) and planar cross-bedded gravel units (Gc). The planar cross-stratified gravels have steeply-dipping foresets (30-40°) and form distinctive clinoformal gravel bodies up to 5 metres in thickness (e.g. at 80 m position, Fig. 2.9).

Unit C consists of interbedded package of poorly-sorted sand and gravel. The unit is truncated by Unit D in the first 120 m of the outcrop and is present only to the southwest of Log 5 (Fig. 2.8). The lithofacies include massive sands and gravels (Sm, Gm), rippled sands (Sr), trough-cross bedded gravelly sands (St) and planar tabular cross bedded gravels (Gc). The individual sub-units are typically about 0.5-4 metres in thickness. The grain sizes ranges from fine sands to medium gravels.

Unit D is a distinctive reddish-coloured poorly-consolidated sandy diamict (Ds) with more well sorted pebbly sand interbeds. The unit is matrix supported and is typically massively bedded with indistinct crude horizontal bedding and infrequent planar cross stratification. The unit's reddish colour derives from the presence of red clays in the matrix, most likely produced by erosion of Queenston Formation shales. Unit D truncates Unit C completely at the northern end of the outcrop and overlies Unit B across an erosive contact.

Unit E is an uppermost, thin (< 1.5 m) sandy gravel that begins about 50 metres into the profile (Fig. 2.8). It consists chiefly of poorly-sorted sandy gravel and lacks discernible bedding structure.

2.4.2 GPR Results

Seven distinctive subsurface radar facies were identified in the 3-D GPR data (G-f1 – G-f7) and four in the outcrop GPR data (O-f1 – O-f4) using Neal's (2004) criteria (Figs. 2.8, 2.9). Six radar surfaces were recognized within the subsurface (G-s1 – G-s6) and three in the outcrop (O-s1 – O-s3). Radar surfaces were defined by high amplitude reflection events that bound one radar facies from another and were most easily identified in the 50 MHz data. The outcrop surfaces were identified within the radar data and then compared against actual outcrop data and photos to evaluate how well the GPR was able to resolve bounding surfaces. Although smaller surfaces (< 1 metre) could not be resolved in the 50 MHz data, bounding surfaces larger than this were identified in both the GPR and outcrop data. This information was then used as an analogue to aid in delineating the bounding surfaces within the grid data. The radar surfaces and their internal radar facies in turn allowed two major reflection (RP-1, RP-2) packages to be identified.

Both the 50 and 250 MHz data were used to characterize the radar facies and radar surfaces for the 3-D GPR surveys, while only the 50 MHz data were used for the outcrop study due to the superior penetration of this frequency in the outcrop (Fig. 2.9). Within the subsurface, the 50 MHz frequency provided the best overall imaging of major bounding surfaces (5^{th} order), separating radar facies (Fig. 2.10), while the 250 MHz data provided finer resolution of intra-element bedding structures (Fig. 2.11). Table 2.1 provides a reference key to determine which colour represents a particular outcrop of radar surface. The colour used to identify each surface is consistent through all figures.

Figure 2.9: 50 MHz GPR profile collected along top of outcrop and overlaid with portion of radar profile Line 10 from the pit base (Grid 1, Line 10) (NW to SE orientation). Borehole MW-22 lithology and geophysical logs (conductivity, magnetic susceptibility and gamma) shown for comparison. Five radar facies (O-f1- O-f4) and bounding radar surfaces (O-s1-O-s3) were identified in outcrop. Clinoformal reflectors in O-f2 record lateral accretion of gravel bars macroforms. Six radar facies (G-f1 – G-f6) were identified in the 3-D GPR survey data (Line 10).

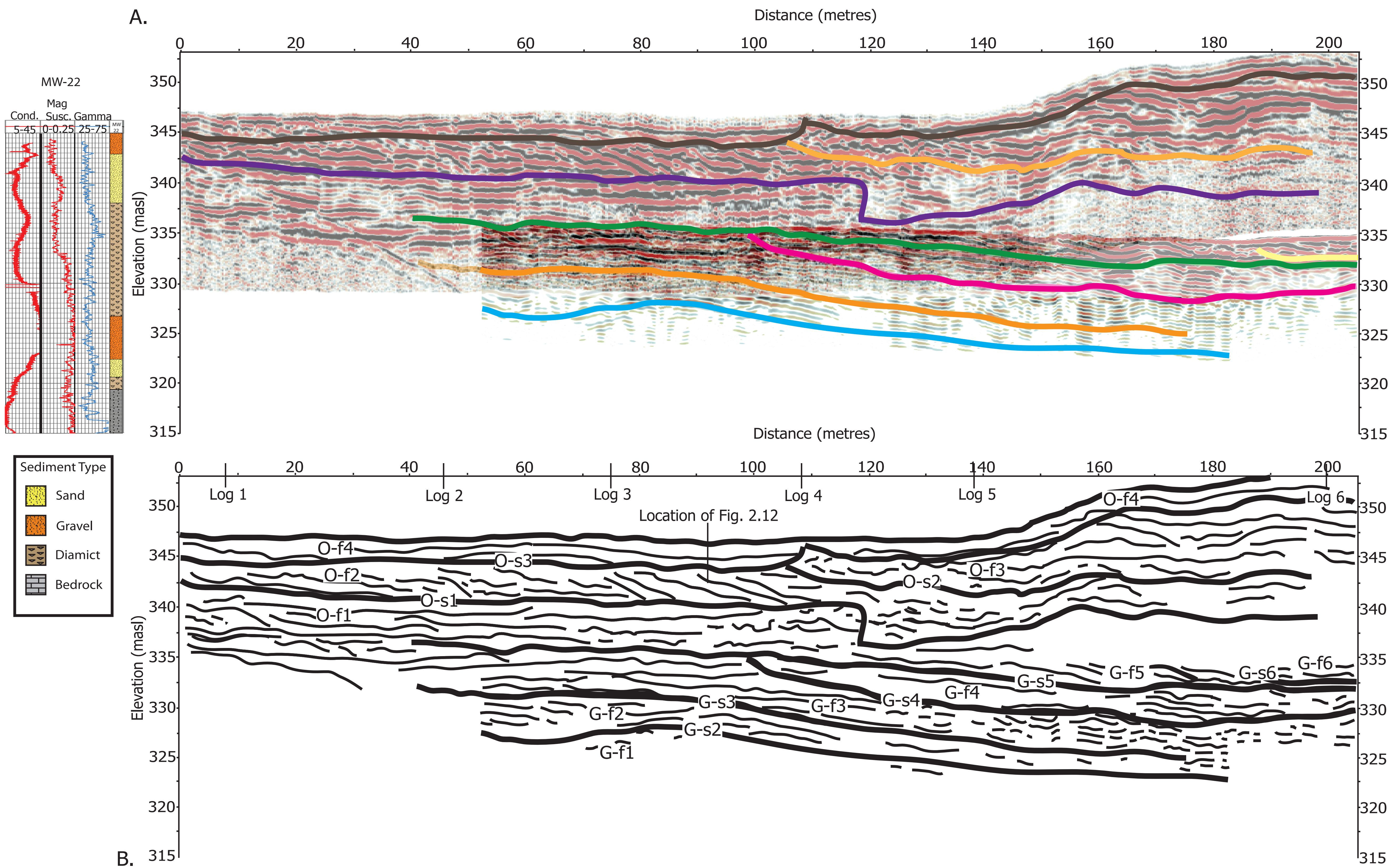
A.
Distance (metres)
Elevation (masl)
MW-22
Cond.
Mag Susc.
Gamma
5-45
0-0.25
25-75
Sediment Type
Sand
Gravel
Diamict
Bedrock
B.
Log 1
Log 2
Log 3
Log 4
Log 5
Log 6
Location of Fig. 2.12
O-f4
O-s3
O-f2
O-s1
O-f1
O-s2
O-f3
G-f5
G-s6
G-f6
G-s5
G-f4
G-s4
G-f3
G-s3
G-f2
G-s2
G-f1

Figure 2.10: 50 MHz GPR profile Line 0 (Grids 1 and 2). A. Radargram with major 5th order bounding surfaces traced. B. Interpreted reflection patterns and radar facies (G-f1-G-f7). Six crossing profiles showing radar facies perpendicular to along-line direction of NW – SE.

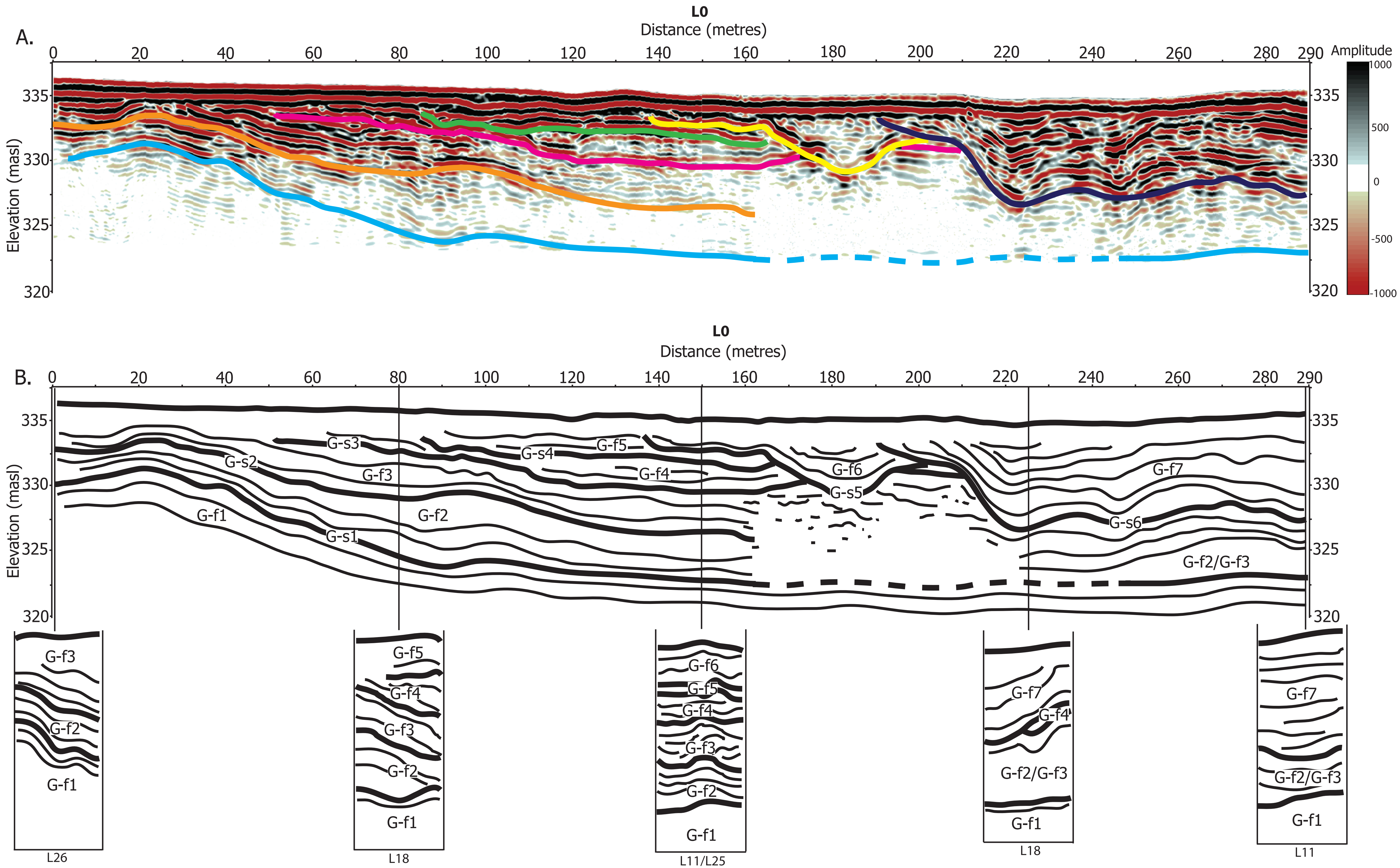
A.
L0
Distance (metres)
0 20 40 60 80 100 120 140 160 180 200 220 240 260 280 290
Elevation (masl)
335 330 325 320
Amplitude
1000 500 0 -500 -1000
B.
L0
Distance (metres)
0 20 40 60 80 100 120 140 160 180 200 220 240 260 280 290
Elevation (masl)
335 330 325 320
G-s3
G-s4
G-f5
G-s2
G-f3
G-f4
G-f6
G-s5
G-f7
G-f1
G-f2
G-s1
G-s6
G-f2/G-f3
G-f3
G-f2
G-f1
L26
G-f5
G-f4
G-f3
G-f2
G-f1
L18
G-f6
G-f5
G-f4
G-f3
G-f2
G-f1
L11/L25
G-f7
G-f4
G-f2/G-f3
G-f1
L18
G-f7
G-f2/G-f3
G-f1
L11

Figure 2.11: A. 250 MHz GPR profile Line 0 (Grids 1 and 2). Note the profile depth extent equates to the top 5 metres of the 50 MHz profile due to decreased penetration of the 250 MHz system. The radargram demonstrates the trade-off between depth penetration and radar resolution. B. Interpreted reflection patterns and radar facies (G-f2-G-f7). The radar surfaces (G-s2 – G-s6) are based on 50 MHz radar interpretation.

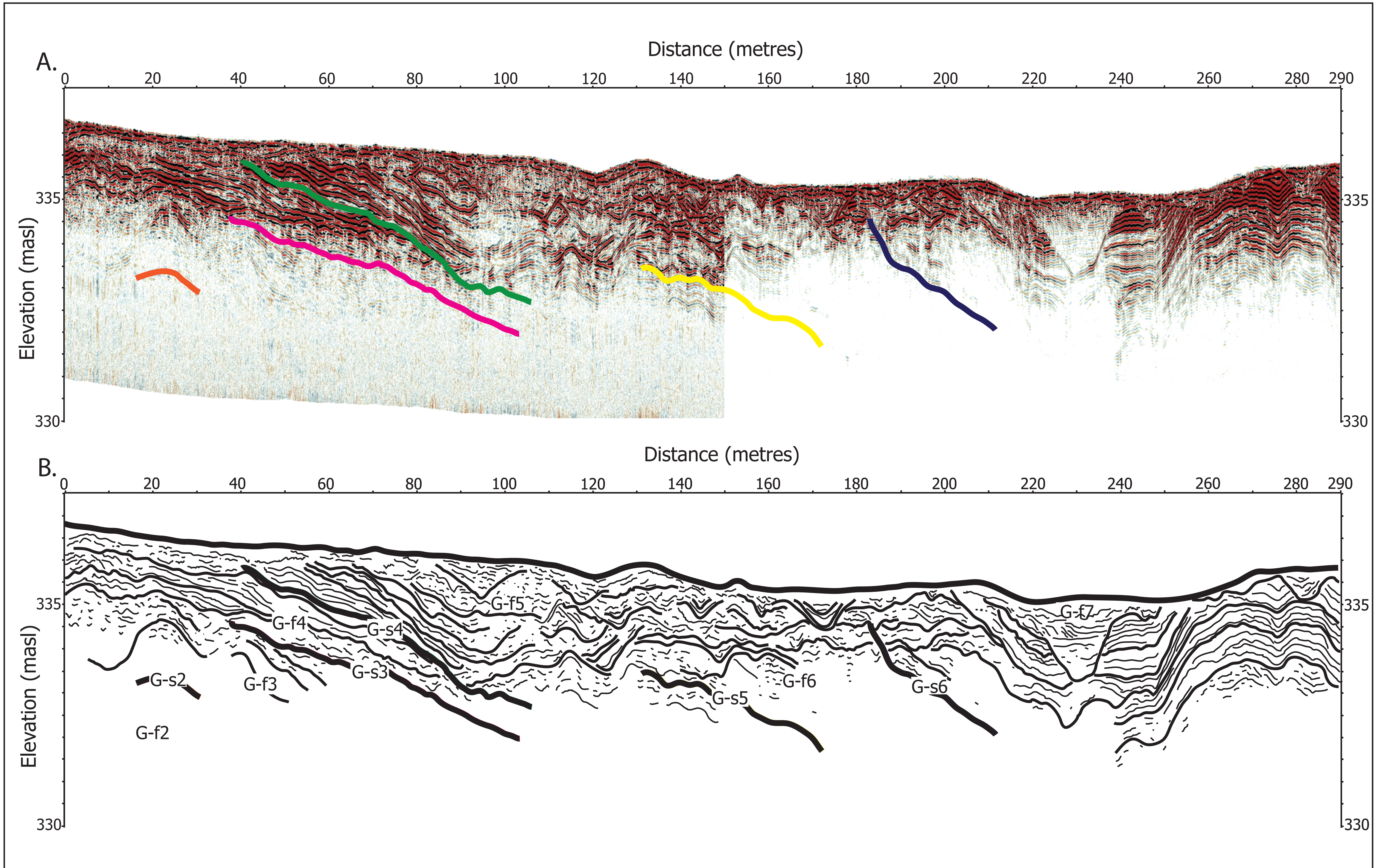
A.
Distance (metres)
0 20 40 60 80 100 120 140 160 180 200 220 240 260 280 290
Elevation (masl)
335
330
B.
Distance (metres)
0 20 40 60 80 100 120 140 160 180 200 220 240 260 280 290
Elevation (masl)
335
330
G-s2
G-f2
G-f3
G-f4
G-s3
G-s4
G-f5
G-s5
G-f6
G-s6
G-f7

Table 2.1: Key defining colour scheme in figures 2.9 – 2.11 in both the outcrop and subsurface data. The colour of each surface remains consistent throughout all of the profiles (e.g. light blue represents G-s1 in all profiles, where visible).

Surface	Colour representation in profiles
G-s1	
G-s2	
G-s3	
G-s4	
G-s5	
G-s6	
O-s1	
O-s2	
O-s3	

2.4.2.1 Outcrop GPR

The interpreted outcrop radar facies are shown in a panel diagram in Fig. 2.9. The panel diagram combines the 50 MHz radargrams from the outcrop and 3-D survey (Line 10). Four distinct radar facies (O-f1 - O-f4) were identified by comparison with the outcrop photos and lithofacies logs.

Radar facies O-f1 comprises a thick package (> 5 m) of moderately continuous, horizontal, planar reflectors that are mostly parallel to one another. The facies is bounded below by subsurface radar surface G-s5 and is concordant with the underlying radar facies G-f3 and G-f4. O-f1 has a concordant upper boundary with radar surface O-s1. This radar facies corresponds with the lithofacies assemblage Unit A (Fig. 2.8).

Radar facies O-f2 consists of clinoformal and wavy reflectors with relatively high reflection amplitudes. The clinoformal reflectors are sub-parallel or in some cases show an oblique geometry. The clinoforms are best developed between 60 to 100 m on the outcrop profile and dip at about 25-40° to the southeast (Fig. 2.9, 2.12). The clinoforms show a toplap condition with the upper bounding surface (O-s3) and a downlap with the lower boundary (O-s1). At 120 m along the profile, O-f2 sharply truncates underlying radar facies O-f1 across a highly erosive boundary. Radar facies O-f2 corresponds with Unit B stratified gravels (Fig. 2.8).

O-f3 consists of a thick package (up to 8 m) of continuous, moderately sinuous sub-parallel reflectors. O-f3 is truncated below radar surface O-s2 and is not present in the first 110 m of the profile (Fig. 2.9). O-f3 is equivalent to the Unit C sediments (Fig. 2.8)

O-f4 is a thin package of continuous, horizontal parallel reflectors with a 'draped geometry' that parallels the surface topography (Fig. 2.9). The lower bounding surface of this facies (O-s3) is a sharply erosive boundary, as it is truncates and discordant with the reflection patterns in the underlying radar facies O-f2 and O-f3. Radar facies O-f4 corresponds with the lithofacies assemblages D and E (Fig. 2.8).

Figure 2.12: A. Portion of 50 MHz outcrop radargram showing GF element. B. Outcrop photograph showing high-angle gravel foresets dipping to southeast. Location shown in Fig. 2.10. The difference in scales from A. to B. accounts for the seemingly higher angle of the foresets in Figure A.

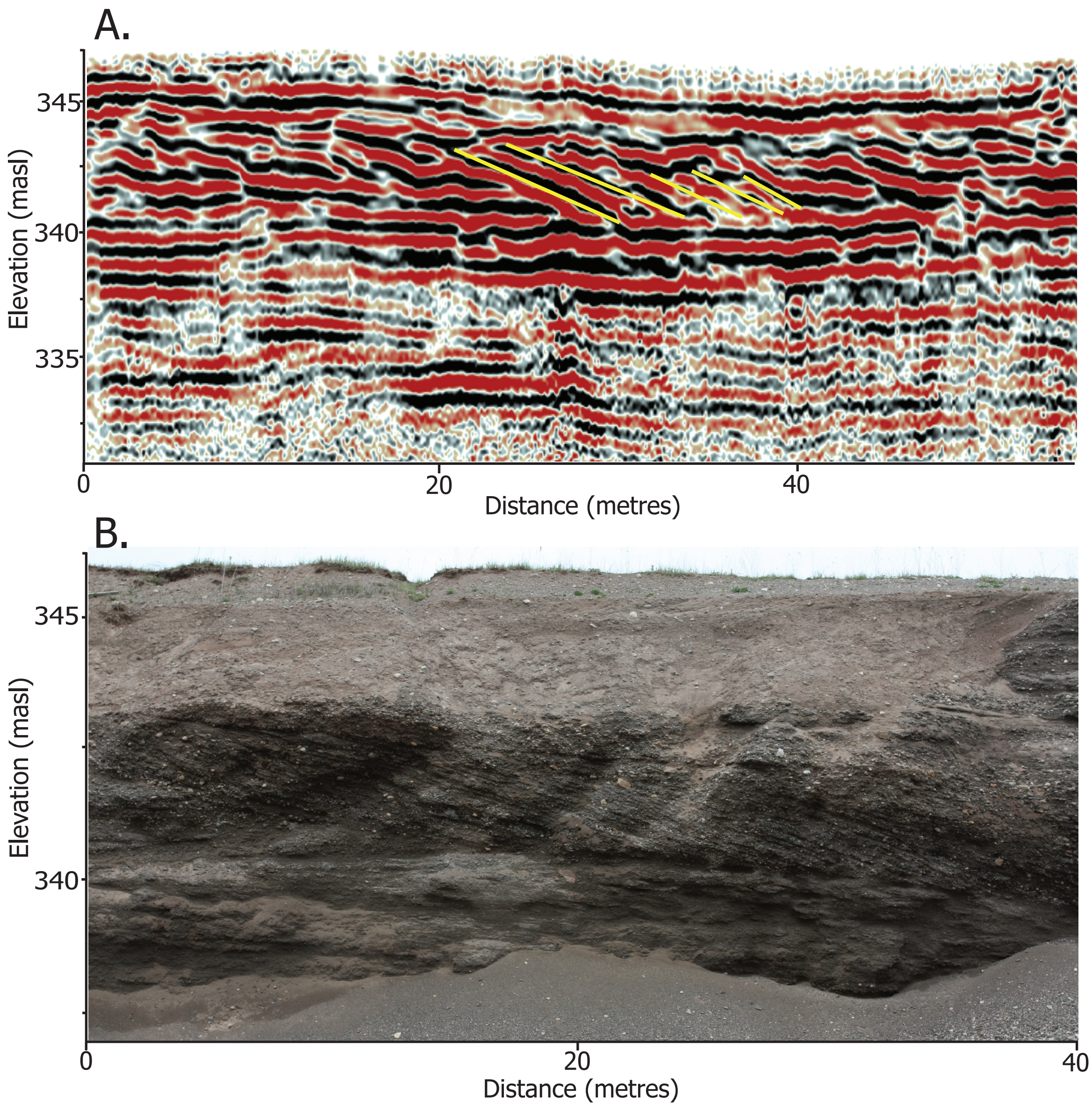
A.
345
340
335
Elevation (masl)
0
20
40
Distance (metres)
B.
345
340
Elevation (masl)
0
20
40
Distance (metres)

2.4.2.2 3-D GPR

The subsurface radar facies were interpreted by picking of radar surfaces in successive profiles extracted from the 3-D volumes (Fig. 2.6). Because of the large amounts of data, not all of the profiles can be reproduced in this paper and only two representative profiles are shown in Figures 2.10 and 2.11 for the 50 and 250 MHz frequencies, respectively. Both profiles were extracted from the first line in the 3-D volume, corresponding to Line 0 (Fig. 2.4). Seven distinct radar facies were identified using the 50 MHz data, which provide a depth of penetration of about 15 m below the pit base. The 250 MHz data, in contrast, provide only about 6-8 m of profile depth but are much higher resolution (Fig. 2.11)

Radar facies G-f1 comprises low amplitude parallel to sub-parallel reflectors with a planar to wavy geometry. Its lateral continuity is undeterminable due to a loss of penetration below 14 m. The reflector dips range from 0° to about 10° towards the southeast. G-f1 is not recorded within the 250 MHz data, as it sits below the maximum penetration depth. The lower bounding surface of G-f1 was not imaged but its top is defined by radar surface G-s1. It is the deepest and most relatively continuous reflector with a concave upward geometry. Gs-1 has a complex surface topography as shown in the interpolated radar surfaces in Figure 2.13. At the north end of Grid 1 the unit dips steeply from west to east (Line 26) and changes to a moderate northeast to southwest dip along the profile (Line 18) (Fig. 2.10). The dip continually steepens as the surface is followed south.

Figure 2.13: Interpolated radar reflection surfaces defining major 4^{th} and 5^{th} order bounding surfaces. A. View from southwest. B. Viewed from northeast. G-s1 – G-s4 represent the major 4^{th} order clinoformal surfaces defining gravel packages that dipping southeast towards135º. G-s5 and G-s6 define the bases of major channel trending northeast to southwest that truncates the underlying boundaries G-s4 and G-s3.

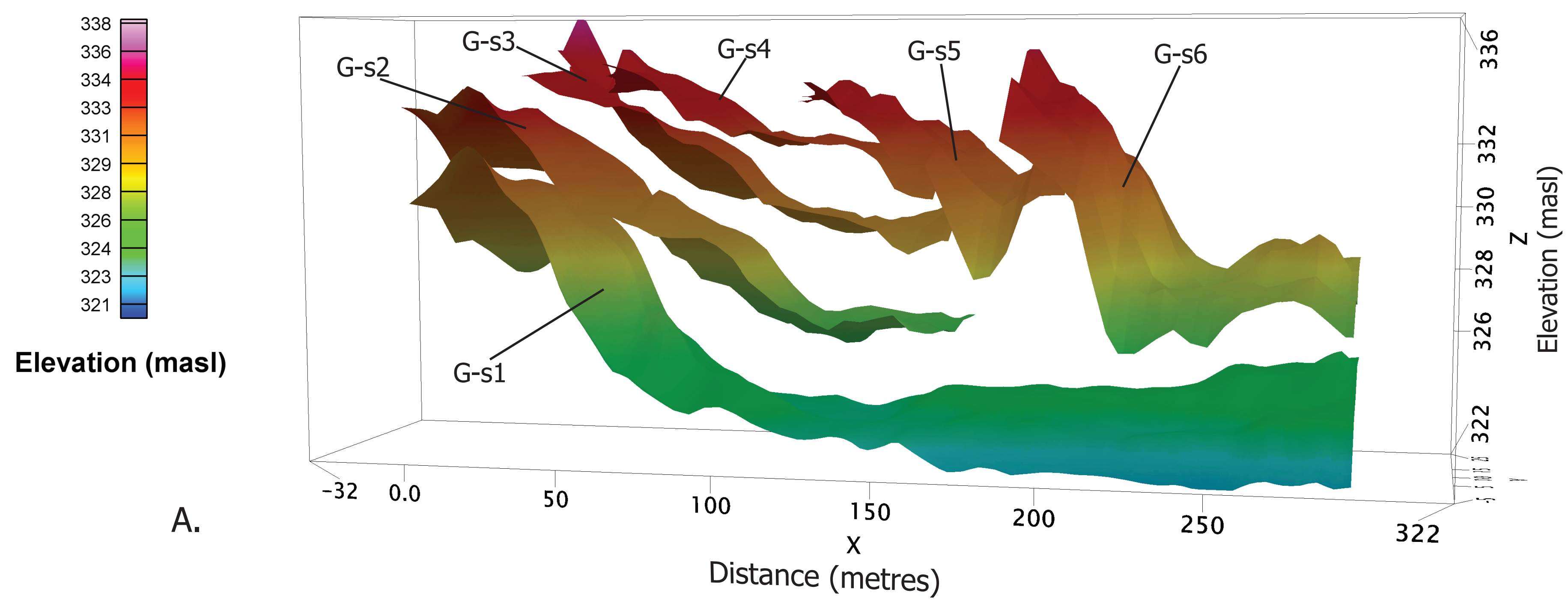
338
336
334
333
331
329
328
326
324
323
321
Elevation (masl)
G-s1
G-s2
G-s3
G-s4
G-s5
G-s6
-32
0.0
50
100
150
200
250
322
X
Distance (metres)
336
332
330
328
326
322
Z
Elevation (masl)

A.

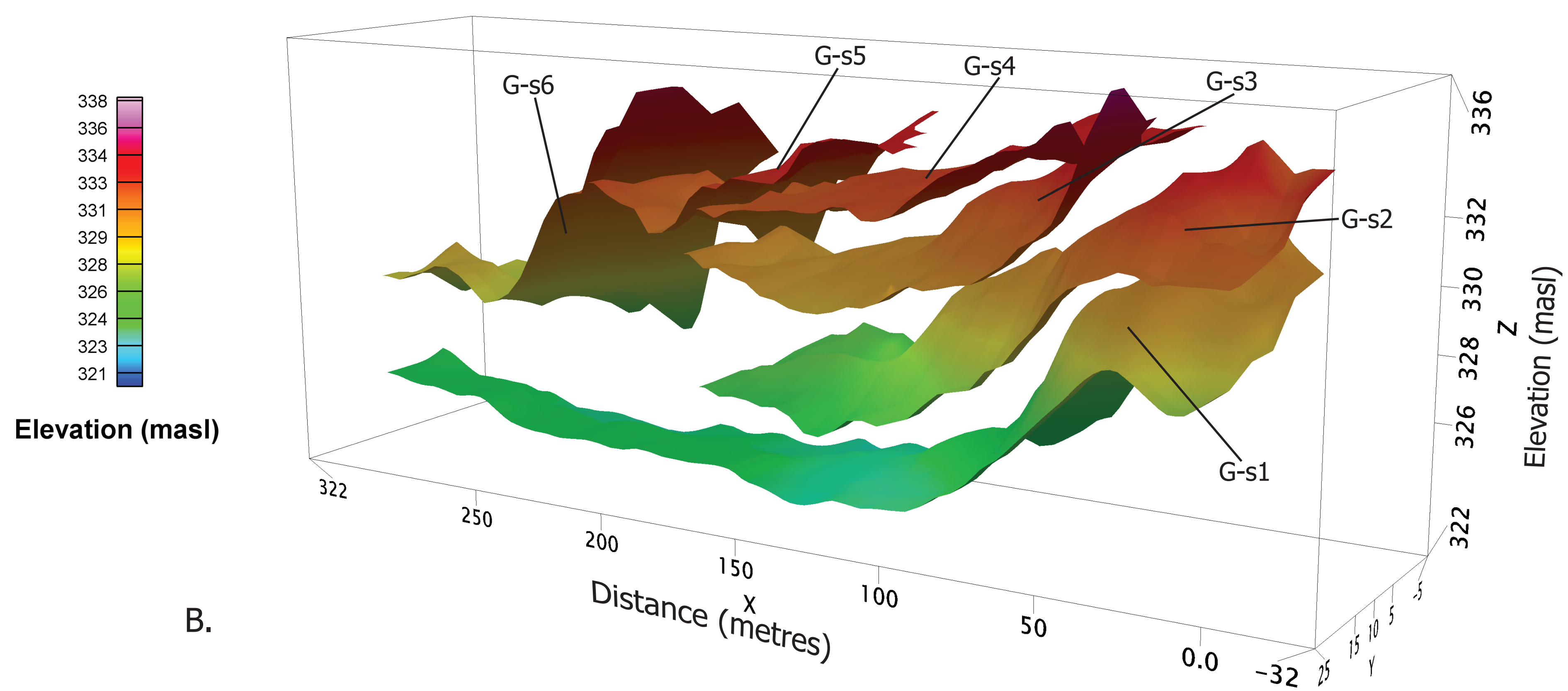
338
336
334
333
331
329
328
326
324
323
321
Elevation (masl)
G-s6
G-s5
G-s4
G-s3
G-s2
G-s1
322
250
200
150
100
50
0.0
-32
X
Distance (metres)
336
332
330
328
326
322
Z
Elevation (masl)
Y

B.

G-s1 forms a broad channel feature that erosively truncates the underlying radar facies G-f1 (Fig. 2.10).

G-f2 consists of low amplitude continuous reflectors with a planar to wavy geometry. The reflectors are parallel to sub-parallel and the dip 0° to 15° in a southeast direction. G-f2 is not imaged in the 250 MHz data. G-f2 is bounded above by G-s2, a continuous concave up radar surface with an undulating reflection geometry (Fig. 2.13).

G-f3 is a package of planar to wavy reflectors that are parallel to sub parallel. The reflectors dip from 0° to about 10° to the southeast. G-f3 is erosively truncated by the overlying radar surface G-s3. The G-s3 radar surface has an overall concave upward geometry, paralleling that of G-s2 and complex surface topography (Fig. 2.13).

Radar facies G-f4 and G-f5 consist of continuous, sub-parallel to parallel reflectors with sub-parallel to wavy geometry as shown in the 250 MHz data (Fig. 2.11). The reflectors in G-f4 dip at a low angle (< 5°) to the southeast and are truncated erosively by radar surface G-s4. Radar facies G-s5 shows a more complex internal reflector pattern, consisting of sinuous, convex and concave reflectors with highly variable dip directions (Fig. 2.10). Sigmoidal and convex up 'dome-shaped' reflection geometries are also common in radar facies G-f5, as shown in the high-resolution 250 MHz images in Figure 2.11.

Radar facies G-f6 and G-f7 are notably different from the underlying radar facies (Figs. 2.10, 2.11). These facies are bounded below by high-amplitude radar surfaces (G-s5, G-s6) that truncate underlying radar facies across a concave-up, channelized erosion surface. The G-f6 facies has moderately continuous, parallel reflectors that conform generally to the concave shape of the Gs-5 surface. The upper portion of the channel fill sequence consists of more discontinuous, complex reflection patterns, including many short wavelength (<0.5-2 m) concave and convex reflections. Radar facies G-f6 and the G-s5 radar surface are both truncated by the channelized G-s6 surface. The G-f7 radar facies consists of laterally continuous reflectors with a sinuous/wavy geometry. In the middle of Grid 2 the crossing profiles for G-f7 show continuous, dipping reflectors trending in the southwest direction.

2.5 INTERPRETATION

2.5.1 Radar Facies

The outcrop and subsurface radar facies were interpreted with reference to lithofacies assemblages and outcrop photos (Figs 2.8, 2.9, 2.12). Radar facies O-f1 corresponds with the Unit A stratified gravelly sand facies (Fig. 2.8). The rippled, planar-bedded and trough-bedded sandy facies of Unit A indicate deposition by traction currents in high-energy fluvial flows (Boggs, 2006). The planar- and trough-cross bedded facies are interpreted to record lower flow regime conditions and the planar-bedded facies as upper-flow-regime plane bed deposits. The planar-parallel reflector geometry of O-f1 indicates overall vertical aggradation of Unit A facies, possibly as channel fill deposits in a braided fluvial system (Miall, 1992; Bridge, 2003). The distinctive coarsening-upwards trend in Unit A (Fig. 2.8) suggests that the flow regime was shifting to higher energy levels as a result of the migration of the braid plain channels or due to increasing discharge in the river system.

Radar facies O-f2 corresponds with the Unit B stratified coarse sandy gravels (Fig. 2.8, Fig. 2.9). This radar facies is characterized by packages of high-angle (25-40°) clinoformal reflectors (Fig. 2.12). The clinoforms record the presence of large planar cross-beds in Unit B and are indicative of either the growth of small Gilbert-type deltas in standing water, or the downstream migration of gravel bar macroforms in a high-energy braided river system (Miall, 1996). The scale of the crossbed co-sets (>3 m) would favour subaqueous deposition, for example in a fan-delta prograding into a shallow proglacial lake.

Radar facies O-f3 is coincident with the interbedded sand and gravels of Unit C (Fig. 2.8, 2.9). The presence of abundant current ripples, planar and trough-cross-beds in Unit C indicates deposition in a high-energy fluvial system. The facies characteristics and reflection geometry are similar to that of Unit A/O-f1, suggesting a similar origin as sand-dominated braided river deposits.

Radar facies O-f4 is correlated with the Units D and E in outcrop (Fig. 2.8, 2.9). The distinctive 'draped' geometry of the reflectors in O-f4 and the discordant relationship with underlying radar facies Of-3 indicates a shift in depositional processes. The Unit D facies consist of crudely stratified diamict deposits interbedded with poorly sorted sands and gravels. The facies composition and geometry is consistent with deposition of Units D and E as subglacial till, or as a 'resedimented diamict', formed by debris deposition along a stagnating ice margin (Huggenberger, 1993; Beres et al., 1995; Asprion and Aigner, 1997; Beres et al., 1999; Heinz et al., 2003; Kostic and Aigner, 2007). The geometry of the lower bounding surface O-s3 (Fig. 2.9) indicates substantial erosion of the underlying deposits by the Unit D/E, consistent with subglacial erosion by actively moving ice. The geometry could also be explained by debris flow deposition downslope across a previously-existing subglacial topography (Fig. 2.9).

The subsurface radar facies were interpreted by comparison of the reflector patterns and attributes with the outcrop analogue (Figs. 2.9, 2.10, 2.11). Radar facies G-f1 to G-f5 have similar reflector patterns and geometry, and are characterized by large-scale, low-angle clinoformal reflectors that dip in a southwest to southeast direction (Figs. 2.10, 2.12). The conformity of the bounding surfaces between these radar facies indicates that they were most likely deposited during a single phase of deposition. The planar, horizontal reflectors with moderate strength within are consistent with stratified sand or gravel facies deposited in a high-energy glaciofluvial environment, such as a braided river or a sub-aqueous fan-delta. The low-angle, stacked clinoforms with their concave up geometry (Fig. 2.10) resemble foreset and bottomset gravel bodies in Gilbert-type deltas (Boggs, 2006). The clinoforms dip to the southwest to southeast (180-250°) and are consistent with the deposition of sand and gravels within a prograding lobe of a large sub-aqueous fan delta.

Radar facies G-f6 and G-f7 comprise a package of relatively continuous, concave upwards reflectors overlying a lower bounding surface with a channelized geometry (Fig. 2.10). These radar facies are interpreted to record the development of large nested channel systems that cross-cut the RP-1 deposits. The high amplitude, continuity and frequency of the reflectors indicate that G-f6 and G-f7 are stratified sands and gravels deposited within broad channels that are up to 10 m deep. The G-f6 radar facies is truncated by G-f7, indicating at least two major phases of erosional down-cutting and incision of channels (Fig. 2.10). Within each radar facies a number of smaller 'nested' channels are recognized, indicating multiple episodes of channel migration, down-cutting and infilling. The contoured lower bounding surfaces (G-s5, G-s6) show the channel thalwegs are oriented in a northeast-southwest direction (Fig. 2.13). The dips of reflectors in G-f6 and G-f7 are dominantly towards the southwest, indicating a marked change in paleocurrent direction from RP-1. The fill within G-f6 is likely finer grained than that within G-f7, as indicated by the low reflector amplitudes within G-f6. Radar facies G-f6 and G-f7 are interpreted as second major depositional phase (RP-2; Fig. 2.13) when an outwash plain was cut across the sub-aqueous fan sediments of RP-1 (see Discussion below). The RP-2 sediments represent braided river sediments that infilled a series of broad valleys incised into the surface of RP-1.

2.5.2 Radar Surfaces and Architectural Elements (AE)

Radar surfaces delineate the external form of radar packages (Fig. 2.7) and on a smaller scale they define the bounding surfaces of 'macroforms' and architectural elements (AEs) (Miall, 1983; Boyce and Eyles, 2000; Neal, 2004). Six major radar surfaces were defined within the subsurface (G-s1- G-s7) and three within the outcrop (O-s1 – O-s3) (Figs. 2.9, 2.10, 2.11, 2.14). Radar surfaces identified in the 25 and 50 MHz data represent 5th order and higher bounding surfaces, separating stacked successions of radar facies (Figs. 2.9, 2.10). Lower order 3rd and 4th order surfaces were resolved in the high-resolution 250 MHz, allowing identification of AEs.

The 3-dimensional geometry of the subsurface radar surfaces is shown in Figure 2.13 as a series of colour-shaded structure contour maps. Radar surfaces G-s1 to G-s4 are interpreted as 5th order surfaces, defining a stacked succession of clinoformal radar facies that make up RP-1. The individual surfaces have a complex topography and likely define minor breaks in deposition during the progradation of a sub-aqueous fan delta to southwest and southeast. The RP-1 surfaces are clearly truncated by radar surfaces G-s5 and G-s6, which record a later phase of incision and deposition of outwash deposits in broad channels, with paleoflow directions switching to a more westerly direction (Fig. 2.13).

On a smaller scale, radar surfaces resolved in the 250 MHz data (Fig. 2.11) are useful for defining architectural elements. Five distinctive architectural elements (AE) were identified based on the outcrop data and radar facies and are described in the following sections with reference to Figures 2.14, 2.15 and 2.16. The AEs represent macroforms, which are the building blocks of radar facies and large-scale radar packages (RP-1 and RP-2) (Fig. 2.17).

Figure 2.14: A. Gravel bar (GB) element in 250 MHz longitudinal cross-section (NE – SW), showing steeply-dipping (35-40°) clinoformal reflectors. Note stacked succession of GB elements separated by 4^{th} and 5^{th} order bounding surfaces. B. GB element in 250 MHz cross-section (NW – SE), showing characteristic convex upper bounding surface defining the bar top.

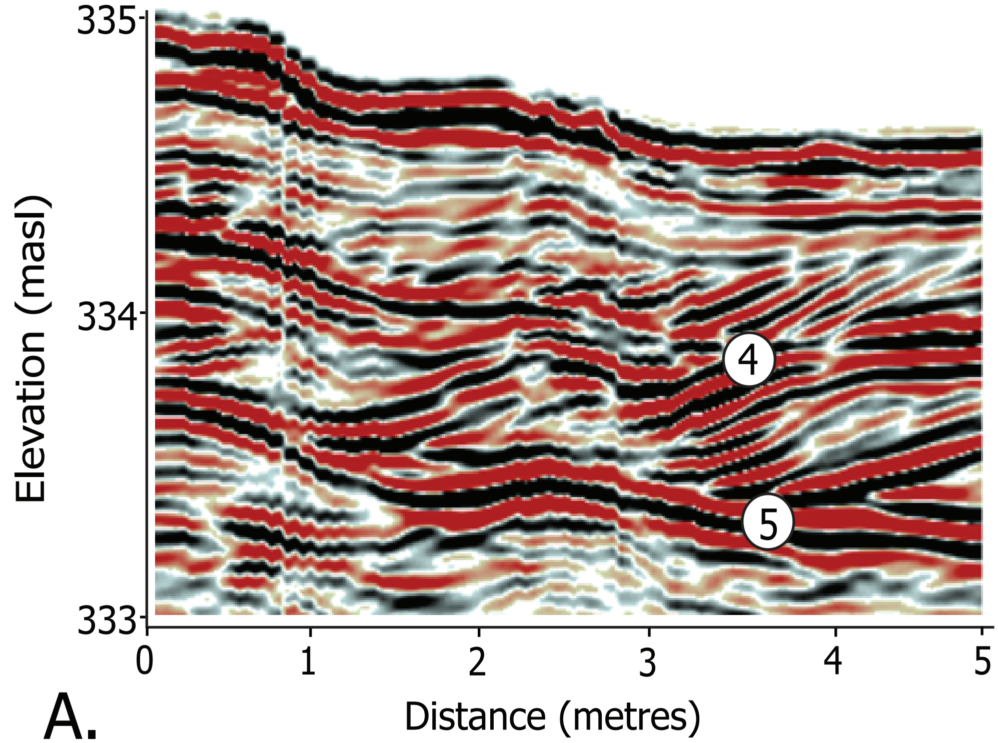
335
334
333
Elevation (masl)
4
5
0
1
2
3
4
5
Distance (metres)
A.

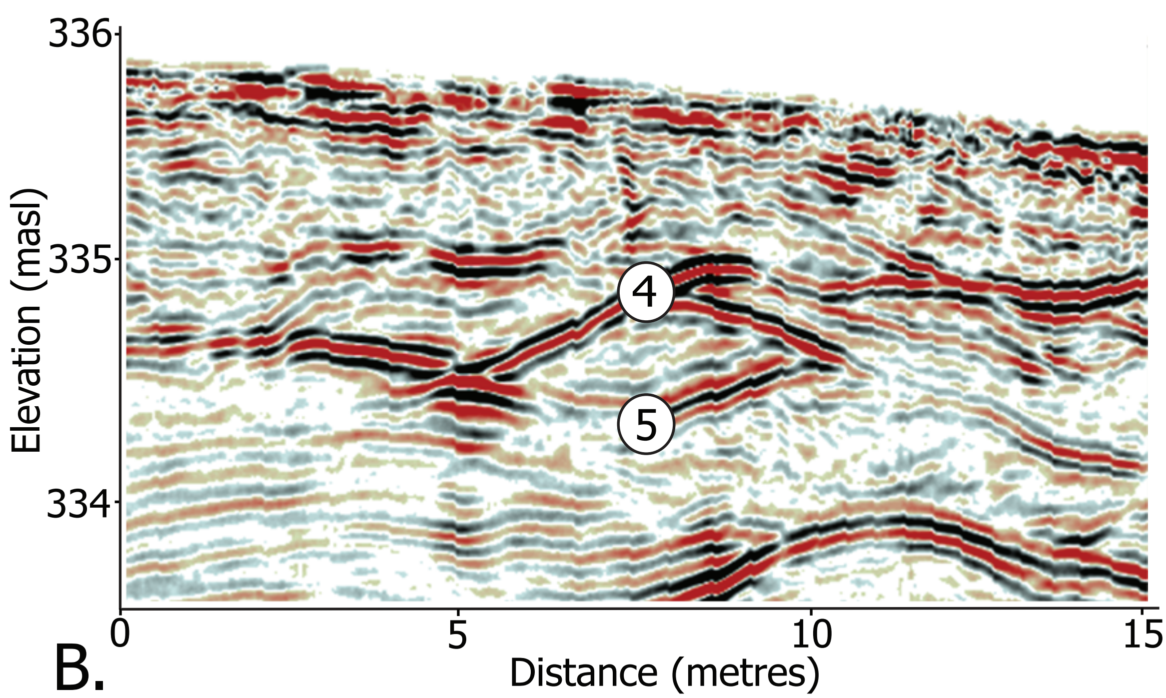
336
335
334
Elevation (masl)
4
5
0
5
10
15
Distance (metres)
B.

Figure 2.15: A. Gravel foreset (GF) element from a longitudinal (NE – SW) 250 MHz cross-section profile showing characteristic scale and steeply dipping (30-45°) reflectors. Note erosive 5th order lower bounding surface and downlap of reflectors onto this surface. An example of a GF element is also shown Fig. 2.15. B. Gravel clinoform (GC) element from a 250 MHz cross sectional (NW – SE) profile, consisting of shallow dipping (<15°) parallel reflectors. GC elements record progradation of sheet-like gravel foresets on a large fan-delta front. Note stacking of elements to form thick wedge-like sand and gravel body (RP-1).

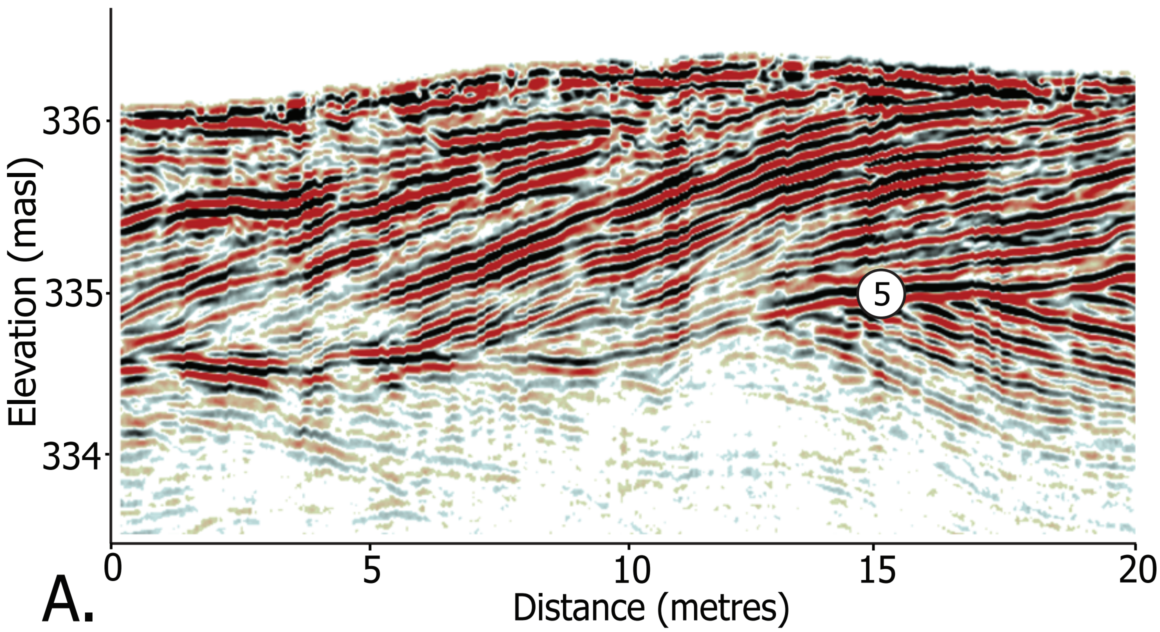
336
335
334
Elevation (masl)
5
0
5
10
15
20
Distance (metres)

A.

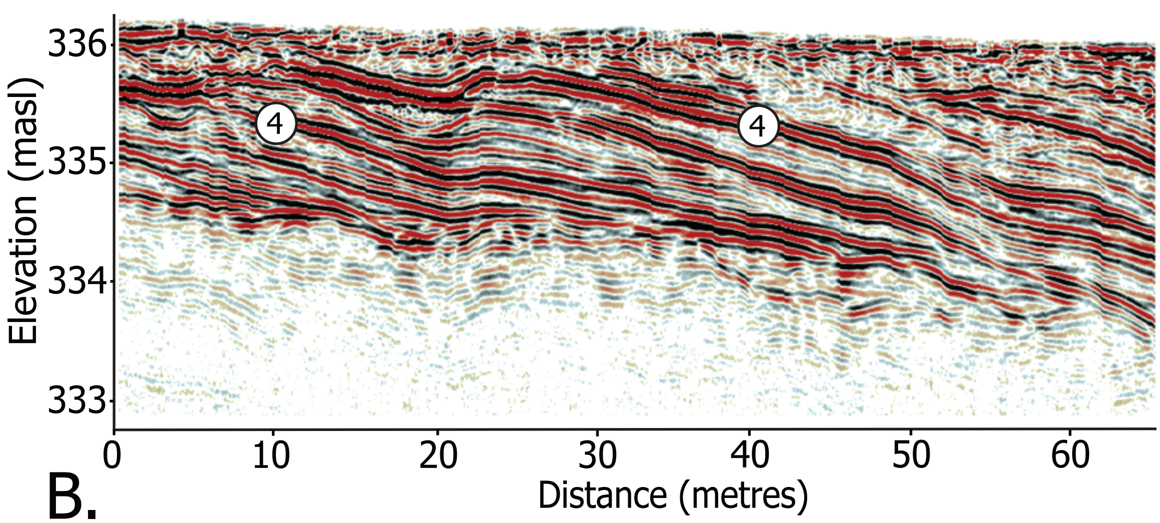
336
335
334
333
Elevation (masl)
4
4
0
10
20
30
40
50
60
Distance (metres)

B.

Figure 2.16: A. 250 MHz longitudinal cross-section (NE – SW) showing vertical aggradation (VA) elements, comprising horizontal, planar reflectors. VA elements are produced by vertical aggradation of sand and gravel facies across a low topography surface within a braided river system. B. Channel (CH) elements from a 250 MHz cross-sectional (NW – SE) profile, defined by trough-shaped lower 5th order surface, which incises and cross-cuts underlying radar facies. CH elements contain both VA and GB elements. CH elements record fluvial incision followed by vertical aggradation/downstream accretion of sand and gravel facies.

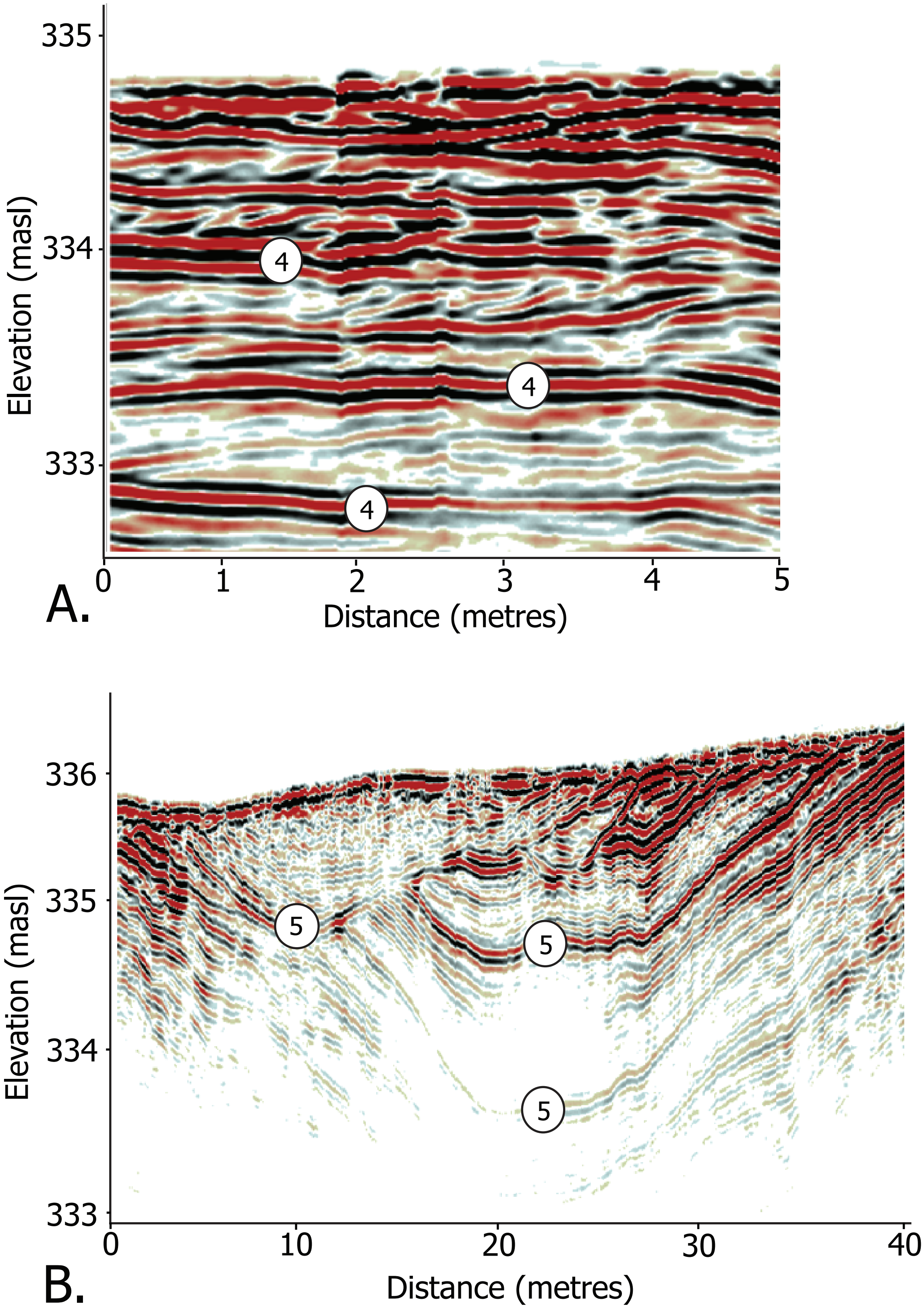
335
334
333
Elevation (masl)
4
4
4
0 1 2 3 4 5
A.
Distance (metres)
336
335
334
333
Elevation (masl)
5
5
5
0 10 20 30 40
B.
Distance (metres)

Figure 2.17: Schematic view of the depositional environments of the architectural elements identified within this study. A. Cross-sectional view of the Gilbert-type delta environment that gravel foreset elements formed in (From Boggs, 2006). B. Overhead view of gravel bars with arrows pointing in direction of flow. C. Cross-sectional view a prograding fan delta that produces the large-scale clinoform elements with arrows showing direction of progradation. D. Stacking of horizontal, planar sands or gravels within a channel in a 3D cross-sectional view. The arrows denote the direction of flow. E. Nested channel formation in a braided river environment in a 3D cross-section. The flow is in the direction of the arrows. Older channels have been eroded and subsequently filled by VA and GB elements. The tough-shape defines the base of each channel.

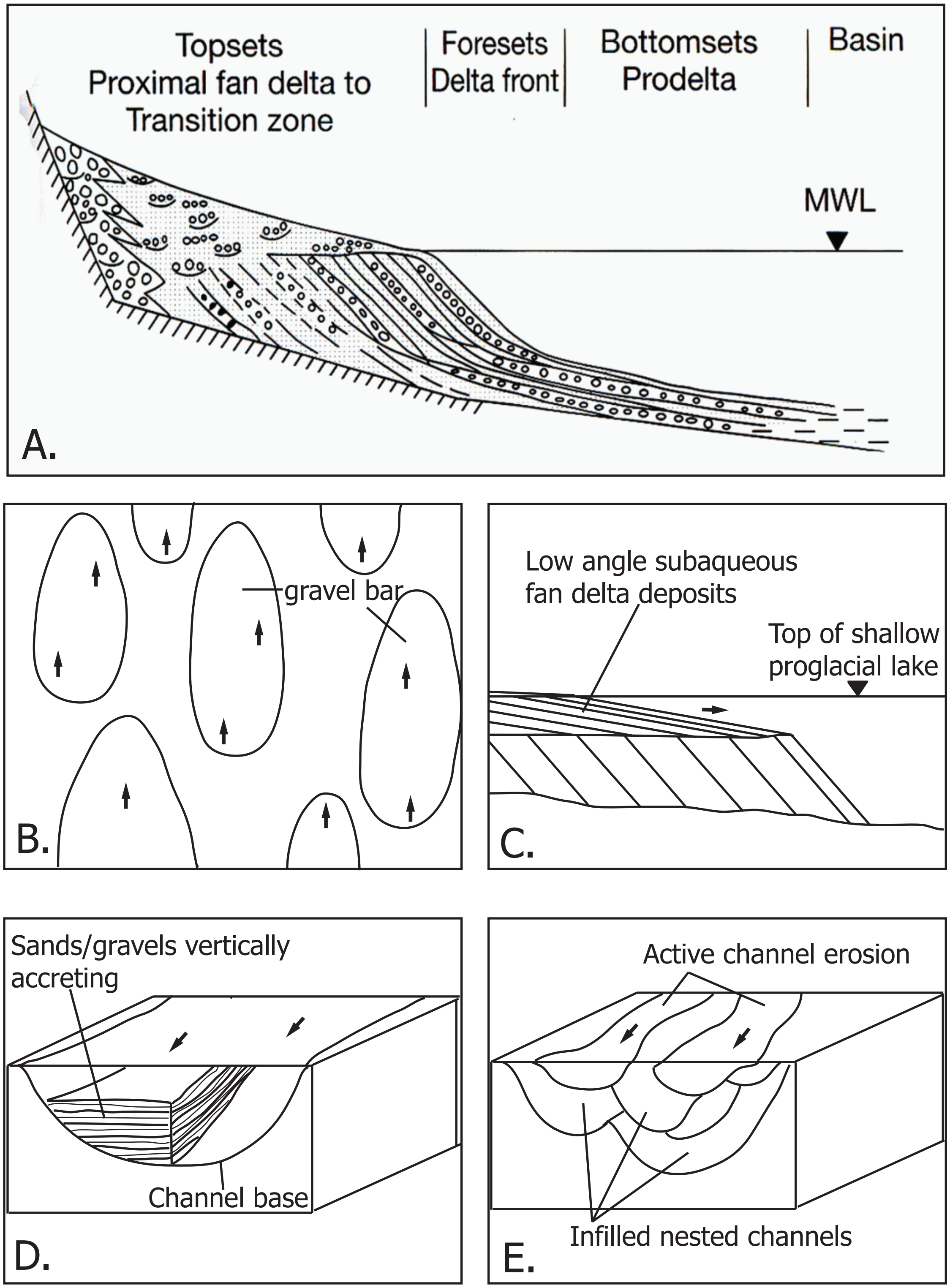
Topsets
Proximal fan delta to
Transition zone
Foresets
Delta front
Bottomsets
Prodelta
Basin
MWL
A.
gravel bar
B.
Low angle subaqueous
fan delta deposits
Top of shallow
proglacial lake
C.
Sands/gravels vertically
accreting
Channel base
D.
Active channel erosion
Infilled nested channels
E.

2.5.2.1 Gravel bar elements (GB)

GB elements are small-scale packages of moderate to steeply-inclined reflectors (30-45°) that have distinctive lens-like geometry in cross-section (Fig. 2.14a, b). In longitudinal profile, GB elements show high-angle (30-45°) oblique and sigmoidal reflectors, recording the progradation of cross-beds within gravel bars (Miall, 1996). In cross-section, GB elements are bounded below by an erosional 5th order surface and distinctive 'domed' convex up 4th order upper surface, defining the gravel bar top. The dimensions of GB elements vary, but they are typically about 3-5 metres in width, 5-10 metres in length and about 1 metre in thickness (Fig. 2.14 a, b). GB elements are equivalent to the downstream accretion (DA) elements of Miall (1983) and are interpreted to record the growth of individual longitudinal bars in a gravelly braided river environment. GB elements are common macroforms in radar package RP-2, where they occur as stacked sequences of amalgamated gravel bars within the channel fill sequences (Fig. 2.10). GB elements are also a common feature of radar facies G-f5 (Fig. 2.11), indicating that the uppermost element of RP-1 was deposited in a outwash plain environment, superposed on the sub-aqueous fan deposits.

2.5.2.2 Gravel foreset elements (GF)

GF elements consist of thick (3-5 m) packages of moderate to steeply-dipping (30-45°) clinoformal reflectors that have a lateral extent of 10's of metres (Figs. 2.15a). GF elements are typically bounded by an erosive 5th order surfaces. The internal reflectors patterns are often sigmoidal or oblique and show a distinctive downlap onto the lower bounding surface. These elements represent large-scale gravel macroforms (typically >10 m in length) produced by the progradation of small Gilbert-type fan-deltas into shallow standing water. The GF elements are one of the most common types in the Wilroy pit (Fig. 2.15).

2.5.2.3 Gravel clinoform elements (GC)

GC elements are large-scale low-angle (<15°) clinoformal reflectors that have length scales of many 10’s to 100’s of metres (Fig. 2.15b; Fig. 2.12). These elements have a sheet-like geometry and are stacked on top of another with conformable boundaries. GC elements are interpreted as large-scale gravel foresets deposited on the front slope of a prograding fan-delta. The GC elements are bounded typically by 4^{th} order surfaces, and are conformably stacked within RP-1 to form a thick, wedge-like sand and gravel body (Fig. 2.10).

2.5.2.4 Vertical aggradation elements (VA)

VA elements are sheet-like in their three-dimensional external form and are bounded by conformable 4^{th} order surfaces (Fig. 2.16a). The bounding surfaces are generally planar-parallel with horizontal reflectors. Lower order surfaces (1^{st} - 3^{rd} order) defining minor erosion surfaces and horizontal planar stratification is present between 4^{th}

order surfaces. These elements are typically 1-2 m in thickness with length scales of 10's of metres. VA elements are composed of interbedded sand or gravel. VA elements are interpreted to record the vertical aggradation of sand and gravel across a pre-existing low topography surface, such as a broad braid plain or sandur. VA elements are a component portion of the channel fill radar facies in radar package RP-2.

2.5.2.5 Channel elements (CH)

CH elements have distinctive broad, trough-shaped external geometry defined by a concave-up reflecting boundary (Figs. 2.7, 2.16b). The lower bounding surface truncates underlying radar facies and is categorized as a 5th order surface. The overlying radar facies lie concordantly atop the lower bounding surface. This element occurs only in radar facies G-s6 and G-s7. CH elements have variable dimensions, but are typically tens of metres in width and 3-5 m in depth. CH elements occur as single channel body or as a series of nest channels (Fig. 2.11). Individual channels frequently cross-cut and have width/depth ratios of about 10. CH elements record the incision and down-cutting of pre-existing sand and gravel facies by fluvial channels, most likely in a high-energy braided river system. The incision phase was followed by infilling of the channels by successive stacking of VA and GB elements.

2.6 DISCUSSION

2.6.1 GPR Resolution

Several studies have employed three-dimensional GPR surveys to image glaciofluvial deposits (Beres et al, 1995; Beres et al. 1999; Kostic and Aigner, 2007; Bayer et al., 2011). However, none of the studies have outlined the importance of incorporating a multi-frequency approach. This study combines the three-dimensional and multi-frequency aspects of GPR surveys and conveys the importance of completing both aspects within complex, highly heterogeneous glaciofluvial environments, especially for hydrogeological studies

The Rayleigh quarter wavelength criterion is used to determine thinnest bed that can be resolved for a given radar frequency (Neal, 2004). The vertical resolution is controlled by the radar impulse wavelength, which is given by:

$$\lambda = \frac{v}{f}$$

where λ = wavelength

ν = radar wave velocity

f = radar impulse frequency

The thinnest bed that can be resolved according to the Rayleigh criterion is ¼ λ. Beds with a vertical thickness greater than ¼ λ will appear as a single reflecting boundary due the interference between the impulse arriving from the bed top and bottom. Because radar systems use a broad band impulse, the frequency is usually estimated as the nominal antenna centre frequency. The vertical resolution can be estimated directly from the radargrams by taking the average separation of consecutive reflecting boundaries (in either depth or time) as representative of the average 'bedding thickness'. Table 2.2 shows the calculated theoretical wavelengths and vertical resolutions compared with those estimated from the radargrams.

Table 2.2: Theoretical and estimated values for the wavelength and resolution of each frequency used in this study (25, 50, 100 and 250 MHz). The theoretical values were calculated using the Rayleigh quarter wavelength criterion, with a velocity of 10 cm/ns. The estimated vertical resolution values were determined from the radargrams.

Frequency (MHz)	λ (m)	¼ λ (m)	Estimated Radargram Vertical Resolution (m)
25	4	1	1.58
50	2	0.5	0.99
100	1	0.25	0.4
250	0.4	0.1	0.18

A sample calculation for the theoretical vertical resolution of the 250 MHz frequency, as shown below, yields a value of 0.1 m. A velocity value of 10 cm/ns was used in the calculation, as this was the approximate radar wave velocity determined by diffraction curve fitting.

$$\lambda = \frac{v}{f}$$

$$\lambda = \frac{10\ cm/ns}{250\ MHz}$$

$$\lambda = \frac{1.0*10^8 m/s}{2.5*10^8\ Hz}$$

$$\lambda = 0.4\ \mathrm{m}$$

$$\lambda\ ¼ = 0.4\ \mathrm{m}/4 = 0.1\ \mathrm{m}$$

Table 2.2 shows that the estimated radargram vertical resolution is lower than the theoretical value for all four frequencies. This is due to the decrease in attenuation effects and low-pass characteristics of the subsurface. The vertical resolution is also a direct function of the dielectric constant of the medium, as it is dependent on the radar wave velocity (Bayer et al., 2011). The Rayleigh quarter wavelength criterion is only a 'ballpark' estimate as it assumes that the sediment being penetrated is of a constant thickness, type, etc. (Grasmueck et al., 2005). Changes in sediment dielectric properties can cause the actual resolution to be much less than what is anticipated. The resolution of radargram also decreases with depth, due to loss of high frequencies and attenuation of the radar amplitude; as the pulse penetrates through the ground it becomes attenuated selectively such that lower frequencies are enhanced and the vertical resolution is decreased with depth.

The 50 and 250 MHz frequencies were best suited for this project. The 50 MHz provided deeper penetration and resolved the higher order bounding surfaces, while the 250 MHz unit allowed for the upper five metres of the subsurface to be mapped in detail and gave rise to a level of resolution which was unattainable with the 50 MHz unit. As shown in table 2.2, the actual resolution of the 50 MHz unit is roughly 1 metre. This means that features smaller than 1 metre are undetected and not seen within the radargram. Lower order surfaces (0^{th} – 3^{rd}) are generally smaller than the 1 metre threshold and will likely be missed by the 50 MHz unit. Therefore, it is important to employ a higher frequency unit to detect these smaller order surfaces. Table 2.2 shows that the 250 MHz unit has a resolution of about .18 metres, which would be able to detect these lower order surfaces and resolve their geometry. The trade-off is that the 250 MHz cannot detect the full extent of the higher order surfaces due to the lack of penetration. Therefore, both the 50 and 250 MHz units should be utilized to examine the subsurface during a GPR study to ensure that both high and low order bounding surfaces are fully resolved: failure to do so could result in an incomplete dataset, which would lead to an incorrect hydrogeological model of the subsurface.

Beyer et al. (2011) and Comunian et al. (2011) identified the importance of defining sedimentary structures on a metre and decimeter scale, as subsurface features of this scale (e.g. sand and gravel lenses) can represent important preferential groundwater flow paths. This study demonstrates that in addition to the need for high-frequency radar data (e.g. > 250 MHz), low frequencies (e.g. 25 MHz) are required for imaging of large-scale reflecting surfaces that bound thick, coarse-grained gravel beds, which are likely to have a strong control on flow patterns at a site scale (Anderson, 1989). Higher frequency units are unable to identify the large, 5th order surfaces due to their lack of penetration and lower frequency units cannot fully delineate the smaller-scale features that make up architectural elements. Therefore, it is imperative to employ a multi-frequency approach when completing a three-dimensional hydrogeological study.

2.6.2 Depositional History

The depositional history of the Wilroy pit was previously interpreted by Slomka (2011) based on a detailed study of the outcrop lithofacies and architectural elements (Fig. 2.18). She recognized 6 distinctive element associations (EA), which are successions of spatially- and genetically-related architectural elements deposited during single depositional cycle (Fig. 2.18). At the base of the succession, EA1 consisted of sands and gravels deposited in braided outwash system with paleoflow directions towards the southwest. EA1 was followed by a phase of deltaic sedimentation (EA2-EA-4; Fig. 2.18) with deposition of sands and gravels in delta front and delta top environments. The paleocurrents during this phase alternated between southwest to southeast. During a final phase, deltaic environments were replaced by gravel-dominated and sandy braided river systems, which deposited sands and gravels in a network of broad outwash spillways (Fig. 2.18).

Slomka (2011) speculated, based on the general southerly direction of paleocurrents, that the source area for the sediments lay to the north, in the Oak Ridges Moraine (Fig. 2.1a). The Oak Ridges Moraine was formed in an interlobate position between the Simcoe and Ontario lobes of the Laurentide Ice sheet during the Mackinaw Interstadial, about 14-13.2 Ka BP (Chapman and Putnam, 1984). As the ice margins receded, large amounts of meltwater and sediment were produced and transported southward in a series of broad glacial spillways along the eastern margin of the Niagara Escarpment (Eynon and Walker, 1974) (Fig. 2.1b). Slomka (2011) did not recognize the uppermost diamict (Halton Till) at the Wilroy pit and concluded that the glaciofluvial sediments were deposited either during the Mackinaw Interstadial (i.e. pre-Halton ice advance) or during the final phase of deglaciation after 13 Ka BP (Barnett, 1991).

Figure 2.18: Conceptual model for Limehouse pit stratigraphy modified from Slomka (2011) with addition of radar packages RP-1 and RP-2.

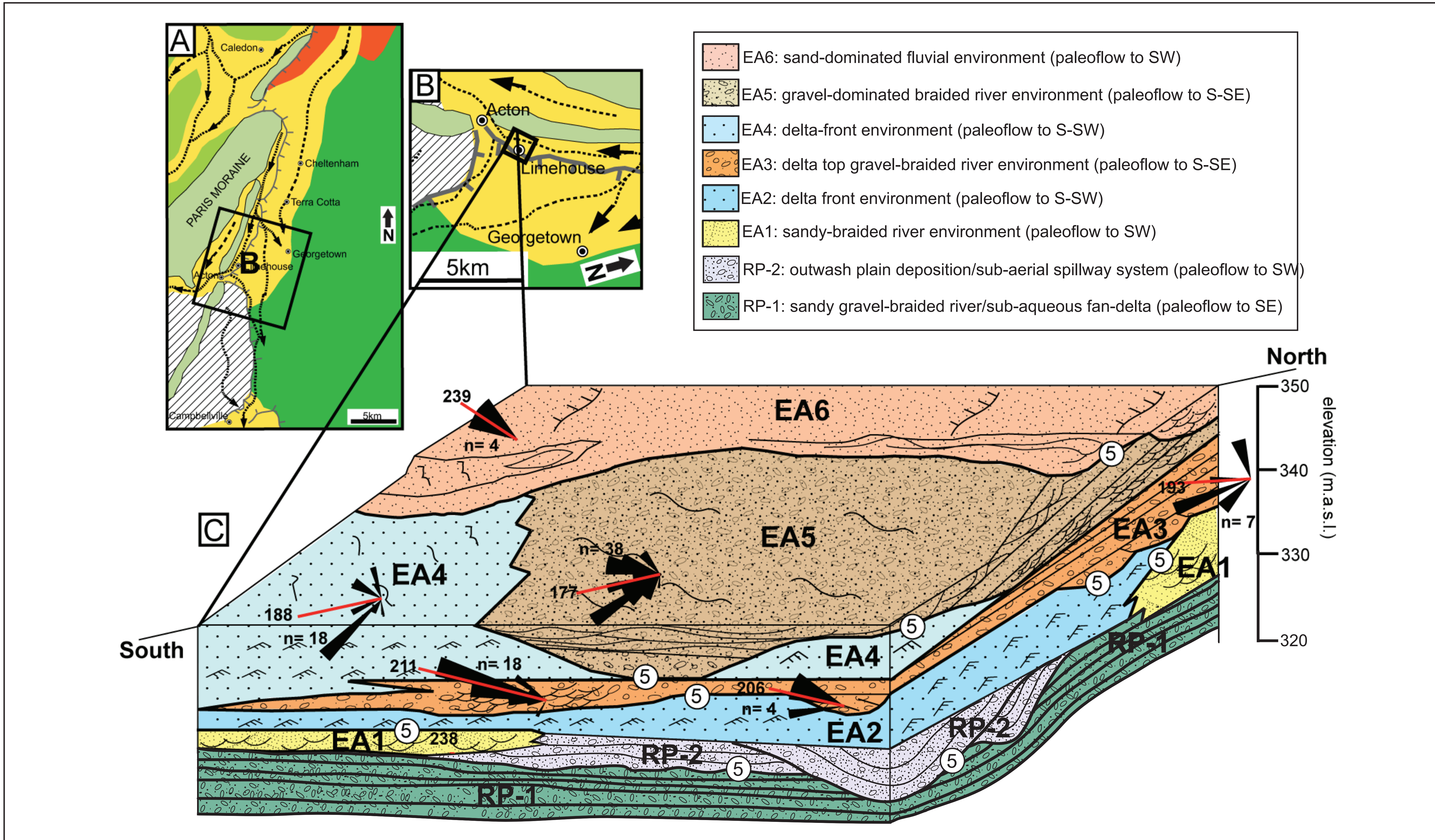
A
Caledon
Cheltenham
Terra Cotta
PARIS MORAINE
Georgetown
Limehouse
Acton
Campbellville
N
5km
B
Acton
Limehouse
Georgetown
5km
N
EA6: sand-dominated fluvial environment (paleoflow to SW)
EA5: gravel-dominated braided river environment (paleoflow to S-SE)
EA4: delta-front environment (paleoflow to S-SW)
EA3: delta top gravel-braided river environment (paleoflow to S-SE)
EA2: delta front environment (paleoflow to S-SW)
EA1: sandy-braided river environment (paleoflow to SW)
RP-2: outwash plain deposition/sub-aerial spillway system (paleoflow to SW)
RP-1: sandy gravel-braided river/sub-aqueous fan-delta (paleoflow to SE)
C
North
South
elevation (m.a.s.l.)
350
340
330
320
239
n= 4
EA6
EA5
n= 38
177
EA4
188
n= 18
211
n= 18
206
n= 4
193
n= 7
EA3
EA1
EA4
EA2
EA1
238
RP-2
RP-1
RP-2
RP-1
5

The conceptual depositional model of Slomka (2011) has been modified with the addition of radar packages RP-1 and RP-2 (Fig. 2.18). RP-1 records a phase of deltaic deposition. The low-angle gravel clinoforms elements (GC) in this package record the active progradation of a fan-delta lobe, most likely into a shallow proglacial lake. Based on the geometry and thickness of the RP-1 package, the lake basin was at least 10-12 m deep (Fig. 2.10). Paleocurrents measured from the dip direction of clinoforms (Fig. 2.13) are oriented at 130-140º, indicating flow to the south-southeast (Fig. 2.18). This flow direction is consistent with paleoflows in EA1, and indicates a source of sediments to the north as interpreted by Slomka (2011). The decrease in clinoform dip angle toward the top of the RP-1 package indicates that the fan-delta front became less steep with time as the lobe prograded. The presence of gravel foreset (GF) and gravel bar (GB) elements in the uppermost radar facies G-f5 of RP-1 also suggests that water depths were declining over time with deposition of small Gilbert-type deltas and gravel bars in shallow water.

During a second depositional phase, the paleoflow switched to a west to southwest direction and the RP-1 deltaic deposits were incised by meltwater channels as recorded by the CH elements of RP-2 (Fig. 2.18). The CH elements are broad channels (depth/width ratios <1:10) most likely formed within a sub-aerial spillway system, as opposed to sub-glacially (e.g. tunnel channels). The channel fills include stacked successions of GB and VA elements, recording the aggradation of the channel deposits over time. The presence of 'nested' and complex cross-cutting channels provides evidence for lateral migration of active fluvial channels on the braid plain surface (Fig. 2.10, 2.11).

2.6.3 Hydrogeological Implications

The results of this study show that the Wilroy pit contains a thick sequence of glaciofluvial sediments, including a highly permeable poorly-sorted sand and gravel facies. The total thickness of the glaciofluvial deposits is estimated to be > 15 m based on the 25 MHz GPR results and core data from the nearby test well MW-22. MW-22 shows the bedrock surface at an elevation of about 319 m.a.s.l. (Fig. 2.9). As the maximum radar penetration was about 12-13 m it is not known whether the sand and gravel deposits rest directly on the fractured limestone bedrock surface or whether the bedrock is capped by a thin diamict unit as indicated by the test well (Fig. 2.9). If the glaciofluvial deposits are in direct hydraulic communication with the fractured upper surface of bedrock, they would have high potential for direct recharge into the Guelph-Amabel Formation aquifer. The results of a recent electromagnetic (EM) survey of the Wilroy pit (Lymburner, 2010) found no evidence for conductive clays or diamict units overlying bedrock at the site and concluded that the glaciofluvial sediments were in contact with bedrock. This conclusion is consistent with the lowermost reflecting boundary in 25 and 50 MHz radar at (320 m.a.s.l.; Fig. 2.10), which most likely represents the overburden-bedrock interface. Prior to development of an artificial recharge project one or more test wells could be completed in the pit base to verify this result.

The radar results show that the glaciofluvial deposits are highly heterogeneous but are devoid of fine-grained materials (silt, clay), which might act as potential aquitards limiting the vertical recharge to underlying bedrock aquifers. Comparison of the outcrop lithofacies with radargrams indicates that changes in radar amplitudes are associated with subtle textural changes in sediments, including changes in grain size and sorting. Although not attempted in this study, future work might investigate the use of radar amplitude attributes for predicting changes in sediment texture and porosity, and as a guide to predicting other key hydrogeologic parameters such has hydraulic conductivity.

The 3-dimensional model of the subsurface architecture of the Wilroy pit deposits provides a useful geologic framework and baseline data for modeling of groundwater flow and surface recharge. The radar surfaces, radar facies and radar packages RP-1 and RP-2 provide a useful framework for defining hydrostratigraphic units when combined with other hydrogeologic data (e.g. pump test data, K estimates). An understanding of the architecture and paleoflow directions is also critical for determining spatial variations in the hydraulic conductivity and porosity. For example, it has been shown that hydraulic conductivities are highly anisotropic in poorly-sorted coarse textured sediments and are often strongly controlled by the preferred orientation of grains. Knowledge of the orientation of more coarse-grained CH fill elements is also critical, as these elements are likely to act as local conduits for groundwater flow and could direct water flow away from the quarry by influencing the lateral flow of the water.

Overall, this study shows that GPR is a key tool to utilize when looking to define areas for artificial recharge basins. The multi-frequency GPR methods employed in this study can be used at other sites being considered as groundwater recharge basins. The GPR data from the Wilroy Pit confirmed that there is no thick aquitard above the bedrock aquifer, which might prevent vertical groundwater recharged. The GPR was also able to define how thick the sediment is within the pit, as a thicker succession of glaciofluvial sediment is better for ensuring less contamination of the groundwater. Since water flows along preferential pathways that are outlined by the paleoflow direction, being able to accurately identify the paleoflow directions using three-dimensional GPR is important for understanding where the water would likely flow to once it percolates below the base of the pit. The GPR identified a system of nested channels in the upper 5 metres of the sediment, which would not have been defined without the use of the 250 MHz unit. These channel systems could change the flow of the water within the pit and redirect the flow in an undesirable direction. Stratigraphic logs, cores and geophysical boreholes cannot define such detailed and important subsurficial three-dimensional data.

Based on the findings of this study, the Wilroy pit and other similar quarries in Halton Hills, once decommissioned, could provide a viable option for artificial recharge system. The sands and gravels housed within the subsurface would allow for the natural percolation of water through them. The Mackinaw Interstadial deposits that make up the sands and gravels are found throughout HR, and thus they should connect from the pit to other areas where water is being pumped. The problem, however, lies in the fact that the pit is still in use on the other side of the road. If the pit were to be decommissioned, the possibility of beginning an artificial recharge site could be seriously discussed. Since there is quite a bit of heavy machinery used in the pits soil contamination levels would also need to be assessed. The connectivity with surrounding streams also needs to be further researched to ensure any aquatic life is not harmed. Any potential for contamination from the nearby Acton Quarry should also be explored.

CHAPTER 3: SUMMARY AND CONCLUSIONS

3.1 CONCLUSIONS

This thesis has presented the results of a multi-frequency GPR study of an active quarry that is being considered for a potential artificial recharge basin. The results shows that 2-D and 3-D GPR surveys are a useful tool in sedimentological and hydrogeological studies, where the top 30 metres of subsurface needs to be imaged. The multi-frequency approach applied here shows that low GPR frequency (25, 50 MHz) units can accurately define major bounding surfaces, while higher frequency units give a detailed view of the upper 5 metres of the sediment. As most hydrogeological studies focus on determining hydrostratigraphic units instead of sub-metre scale details, 50 or 100 MHz units will probably prove most useful.

The three-dimensional architecture of the glaciofluvial deposits in the pit were imaged using four different GPR frequencies and GPR and AEA were used to define the vertical and spatial extent of heterogeneities within the Wilroy Pit of the Limehouse Quarry. Seven radar facies (G-f1 – G-f7) and six radar surfaces (G-s1 – G-s6) were defined within the subsurface, which make up two radar packages (RP-1 and RP-2). RP-1 and RP-2 have distinct paleoflow directions and sedimentation patterns and represent two different depositional events. RP-1 is defined by large-scale, low angle clinoform reflectors that show progradation of gravel macroforms. These foreset bodies are records of meltwater draining to the south-southeast along the edge of the Niagara escarpment. RP-2 records a phase of advance or retreat of the Halton Ice (ca. 13 KA BP) with a change in the paleoflow direction towards the west southwest where RP-1 was eroded in areas and sediments were deposited within these channels.

The most versatile GPR frequency utilized in this study was the 50 MHz unit, as it provided the best overall combination of resolution and depth penetration. Using this frequency major bounding surfaces in the glaciofluvial deposits were delineated to depths of 10-12 m. The trade off for depth over resolution was too great in the 25 MHz unit, while the 250 MHz unit showed very high resolution only in the top 4-5 metres of the quarry sediments. The 100 MHz unit could prove viable as well, although the errors incurred with background noise made the dataset collected for this study less useful. However, high resolution data at the decimeter scale is important for defining preferential flow pathways that otherwise may have been missed by the 50 MHz unit.

3.2 FUTURE WORK

For future 3-D GPR work it would be beneficial to collect the profiles at a much smaller line spacing, especially when using higher frequency systems. The gridding process was hindered by a lack of data from the widely spaced tie lines, which created highly interpolated volumes at higher frequencies. The entire pit area being considered for an artificial recharge basin should be mapped out using a 50 MHz GPR system to properly define radar facies in the pit subsurface. Also, hydraulic properties (such as hydraulic conductivity) within the soil should be mapped using a soil permeameter or in-situ with an air permeameter in order to more accurately assess soil parameters. These measurements would be vital if the quarry were to be seriously considered for artificial recharge. Connectivity between aquifers and streams within the area should be fully identified to determine how, if at all, the streams would react to artificial recharge occurring in the Wilroy pit of the Limehouse quarry. Lastly, measures to ensure that the pit is not contaminated from the large machinery working within it would need to be stringent.

REFERENCES

Allen, J. R. L. (1966) On bed forms and paleocurrents: Sedimentology, 6, 153–190.

Allen, J. R. L. (1983) Studies in fluviatile sedimentology: Bars, bar complexes and sandstone sheets (low-sinuosity braided streams) in the Brownstones (L. Devonian) Welsh Borders: Sedimentary Geology, 33, 237–293.

Anderson, M.P. (1989) Hydrogeologic facies models to delineate large-scale spatial trends in glacial and glaciofluvial sediments. Geological Society of America Bulletin, 101(4), 501-511

Anderson, M.P, Aiken, J.S., Webb, E.K. and Mickelson, D.M. (1999). Sedimentology and hydrogeology of two braided stream deposits. Sedimentary Geology. 129, 187-199.

AquaResource Inc., 2008c. Draft Accepted Integrated Water Budget Report – Tier 2, Credit Valley Source Protection Area. Submitted to Credit Valley Conservation, October 2008.

Aspiron, U. and Aigner, T. (1997). Towards realistic aquifer models: three-dimensional georadar surveys of Quaternary gravel deltas (Signen Basin, SW Germany). Sedimentary Geology, 129, 281-297.

Aspiron, U. and Aigner, T. (1999). Aquifer architecture analysis using ground-penetrating radar: Triassic and Quaternary examples (S. Germany) Environmental Geology, 31(1) 66-75.

Baker, G.S., Plumb, R., Steeples, D.W., Pavlovic, M. and Schmeissner, C. (1999). U.S. Department of Energy Report.

Barnett, P.J. (1992). 'Quaternary Geology of Ontario' *in* Thyrston, P.C., Williams, H.R., Sutcliffe, R.H. and Stott, G.M., eds, Geology of Ontario, Ontario Geological Survey, Special Volume 4, Part 2, Chapter 21, 1011-1088

Bayer, P., Huggenberger, P., Renard, P. and Comunian, A. (2011). Three-dimensional high resolution fluvio-glacial aquifer analog: Part 1: Field study. Journal of Hydrology, 405 (1-2), 1-9.

Benson, A.K. (1995). Applications of ground penetrating radar in assessing some geological hazards: examples of groundwater contamination, faults, cavities. Journal of Applied Geophysics, 33, 177-193.

Beres, M., Green, A., and Huggenberger, P. (1995). Mapping the architecture of glaciofluvial sediments with three-dimensional georadar. Geology, 23 (12), 1087-1090.

Beres, M., Huggenberger, P., Green, A.G. and Horstmeyer, H. (1999). Using two- and three- dimensional georadar methods to characterize glaciofluvial architecture. Sedimentary Geology, 129, 1-24.

Bersezio, R., Giudici, M. and Mele, M. (2007). Combining sedimentological and geophysical data for high-resolution 3-D mapping of fluvial architectural elements in the Quaternary Po plain (Italy), Sedimentary Geology, 202, 230-248.

Boggs, S. Jr. (2006) Principles of Sedimentology and Stratigraphy. Pearson Prentice Hall, Upper Saddle River. 662 pp.

Boniger, U. and Tronicke, J., (2010). Improving the Interpretability of 3D GPR data using Target-Specific Attributes: Application to Tomb Detection. Journal of Archaeological Science, 37, 360-367.

Bowling, J.C, Rodriguez, A.B., Harry, D.L., Zheng, C. (2005). Groundwater, 43(6), 890-903.

Boyce, J.I., Eyles, N. and Pugin, A. (1995). Seismic reflection, borehole and outcrop geometry of Late Wisconsin tills at a proposed landfill near Toronto, Ontario. Canadian Journal of Earth Sciences, 32, 1331-1349.

Boyce, J.I. and Eyles, N. (2000). Architectural element analysis applied to glacial deposits: Internal geometry of a late Pleistocene till sheet, Ontario, Canada. Geological Society of America Bulletin, 112, 98-118.

Brandt, G. (2000). Groundwater Protection and Artificial Recharge – An Integrated Concept. Water Supply, 18(1-2), 547.549.

Brennan, A. N. (2011) "Characterizing the Quaternary Hydrostratigraphy of Buried Valleys using Multi-Parameter Borehole Geophysics, Georgetown, Ontario". [Unpublished M.Sc. thesis]: McMaster University, Hamilton, Ontario. 153p.

Bridge, J.S. (2003) Rivers and floodplains: Forms, processes and sedimentary record. Cambridge, UK, Blackwell Science Ltd. 491pp.

Busby, J.P. and Merritt, J.W. (1999). Quaternary deformation mapping with ground penetrating radar. Journal of Applied Geophysics, 41, 75-91.

Cardimona, S.J., Clement, W.P. and Kadinsky-Cade, K. (1998). Seismic reflection and ground-penetrating radar imaging of a shallow aquifer. Geophysics, 63(4), 1310-1317.

Chapman, L.J. and Putnam, D.F (1984). The Physiography of Southern Ontario, 3rd ed. Ontario Ministry of Natural Resources, Toronto, Ontario. 270pp.

Comunian, A., Renard, P., Straubhaar, J. and Bayer, P. (2011). Three dimensional high resolution fluvio-glacial aquifer analog – Part 2: Geostatistical modeling. Journal of Hydrogeology, 405, 10-23

Costello, W.R. and Walker, R.G. (1972). Pleistocene Sedimentology, Credit River, Southern Ontario: A New Component of the Braided River Model. Journal of Sedimentary Research (formerly Journal of Sedimentary Petrology), 42(2), 389-400.

Davis, J.L. and Annan, A.P. (1989). Ground-penetrating radar for high-resolution mapping of soil and rock stratigraphy. Geophysical Prospecting, 37, 531-551.

Detay, M and Haeffner, H. (1997). The Role of Artificial Recharge in Active Groundwater Management. Water Supply, 15(2), 1-13.

Easton, J.A. (1988). Buried Valleys near Limehouse, Ontario. [Unpublished M.Sc. Thesis]: University of Waterloo, Waterloo, Ontario, 140p

Eyles, N., Eyles, C.H. and Miall, A.D. (1983). Lithofacies types and vertical profile models; an alternative approach to the description and environmental interpretation of glacial diamict and diamictite sequences. Sedimentology, 30, 393-410

Eynon, G. and Walker, R.G. (1974). Facies relationships in Pleistocene outwash gravels, southern Ontario: a model for bar growth in braided rivers. Sedimentology, 21, 43-70.

Ezzy, T.R., O'Rourke, A.J., Huftile, G.J. and Cox, M.E. (2003). Applying ground penetrating radar (GPR) to improve hydrogeological understanding and groundwater modeling within a coastal setting. Tecnologia de la intrustion de agua de mar en acuiferos costeros: paises meditteraneos. 149-156.

Fitzgerald, A. (2009) Ground-Penetrating Radar Study of a Glaciofluvial Aquifer at Limehouse, Ontario. [Unpublished B.Sc. Thesis]: McMaster University, Hamilton, Ontario.

Freeze, R.A. and Cherry, J.A. (1979) Groundwater. Prentice-Hall, Englewood Cliffs, NJ.

Gerber, R.E. and Howard, K. (2002) Hydrology of the Oak Ridges Moraine aquifer system: implications for protection and management from the Duffins Creek watershed. Canadian Journal of Earth Sciences, 39 (9), 1333-1348

Goodman, D., Nishimura, Y., Hongo, H. and Higashi, N. (2006). Correcting for the Topography and the Tilt of Ground-penetrating Radar Antennae. Archaeological Prospection, 13, 159-163.

Goutaland, D., Winiarski, T., Dubé, J.S., Bièvre, G., Buoncristiani, J.F., Chouteau, M. and Giroux, B. (2008). Hydrostratigraphic Characterization of the Vadose Zone of a Glaciofluvial Deposit Underlying an Infiltration Basin using Ground Penetrating Radar. Vadose Zone Journal, 7, 137–139

Ghazi, S. and Mountney, N.P. (2009). Facies and Architectural Element Analysis of a Meandering Fluvial Succession: The Permian Warchha Sandstone, Salt Range, Pakistan. Sedimentary Geology, 221, 99-126.

Grasmueck, M., Weger, R., and Horstmeyer, H. (2004). Three-Dimensional Ground-penetrating Radar Imaging of Sedimentary Structures, Fractures and Archaeological Features at Submeter Resolution. Geology, 32(11), 933-936.

Grasmueck, M., Weger, R., and Horstmeyer, H. (2005). Full-Resolution 3D GPR Imaging. Geophysics, 70(1), 12-19.

Heinz, J., Kleineidam, S., Teutsch, G. and Aigner, T. (2003). Heterogeneity patterns of Quaternary glaciofluvial gravel bodies (SW-Germany): application to hydrogeology. Sedimentary Geology, 158, 1-23.

Holysh, S. (1995). Halton Region aquifer management plan, phase 1, background hydrogeology report. Unpublished report.

Howard, K.W.F., Eyles, N., Smart, P.J., Boyce, J.I., Gerber, R.E. Salvatori, S.L. and Doughty, D. (1995). The Oak Ridges Moraine of Southern Ontario: A Ground-water Resource at Risk. Geoscience Canada, 22 (3), 101-120.

Huggenberger, P. (1993). Radar facies: recognition of facies patterns and heterogeneities within Pleistocene Rhine gravels, NE Switzerland. From: Best, J.L. and Bristow, C.S. (eds), Braided Rivers, Geological Society Special Publication, 75, pp. 163-176.

Huggenberger, P., Meier, E. and Pugin, A. (1994). Ground-probing radar as a tool for heterogeneity estimation in gravel deposits: advances in data-processing and facies analysis. Journal of Applied Geophysics, 31, 171-184.

Huggenberger, P., Rauber, M. and Stauffer, F. (1994). Integration if geophysical and sedimentological information in the stochastic description of inhomogeneities in fluvial gravel deposits. From: Transport and Reactive Processes in Aquifers, Dracos and Stauffer (eds) 1994. Balkema, Rotterdam.

Huysmans, M., Peters, L., Moermans, G. and Dassargues, A. (2008). Relating small-scale sedimentary structures and permeability in a cross-bedded aquifer. Journal of Hydrology, 361, 41-51.

Jol, H.M., Lawton, D.C. and Smith, D.G. (2002). Ground penetrating radar: 2-D and 3-D subsurface imaging of a coastal barrier spit, Long Beach, WA, USA. Geomorphology, 53, 165-181.

Karrow, P.F. (1963) Pleistocene geology of the Hamilton-Galt area. Ontario Department of Mines, Geological Report 16, 68pp.

Karrow, P.F. (1967) Pleistocene geology of the Scarborough area. Ontario Department of Mines, Geological Report 46, 108pp.

Karrow, P.F. (1984) Quaternary stratigraphy and history, Great Lakes-St. Lawrence area. In Geological Survey of Canada Paper 84-10:138-53

Karrow, P.F. (2005), Quaternary Geology of the Brampton Area; Ontario Geological Survey Report 257, 59pp.

Kostic, B. and Aigner, T. (2007). Sedimentary architecture and 3D ground-penetration radar analysis of gravelly meandering river deposits (Neckar Valley, SW Germany). Sedimentology, 54, 789-808.

Leucci, G. and Negri, S. (2006). Use of Ground Penetrating Radar to Map Subsurface Archaeological Features in an Urban Area. Journal of Archaeological Science, 33, 502-512.

Lesmes, D.P., Decker, S.M., and Roy, D.C. (2002). A Multiscale Radar-Stratigraphic Analysis of Fluvial Aquifer Heterogeneity. Geophysics, 67(5), 1452-1464.

Lymburner, J. (2010). EM Conductivity Mapping of Limehouse Quarry, Halton Hills, Ontario. [Unpublished B.Sc. Thesis]: McMaster University, Hamilton, Ontario.

McClymont, A.F., Green, A.G., Streich, R., Horstmeyer, H., Tronicke, J., Nobes, D.C., Pettinga, J., Jocelyn, C. and Langridge, R. (2008). Visualization of Active Faults using

Geometric Attributes of 3D GPR Data: An Example from the Alpine Fault Zone, New Zealand. Geophysics, 73(2), 11-23

Mellet, J.S. (1995). Ground penetrating radar application in engineering, environmental management, and geology. Journal of Applied Geophysics, 33, 157-166.

Meyer, P.A. and Eyles, C.H. (2007). Nature and origin of sediments infilling poorly defined buried bedrock valleys adjacent to the Niagara Escarpment, southern Ontario, Canada. Canadian Journal of Earth Sciences, 44, 89-105.

Miall, A.D. (1985). Architectural-element analysis: a new method of facies analysis applied to fluvial deposits. Earth-Sci. Review, 22, 261-308.

Miall, A. D. (1988a), Architectural elements and bounding surfaces in fluvial deposits: Anatomy of the Kayenta Formation (Lower Jurassic), southwest Colorado: Sedimentary Geology, 55, 233–262.

Miall, A. D. (1988b), Facies architecture in clastic sedimentary basins, *in* Kleinspehn, K., and Paola, C., eds., New perspectives in basin analysis: New York, Springer-Verlag, 63–81.

Miall, A. D. (1992). Principles of sedimentary basin analysis (second edition): New York, Springer Verlag, 668 p.

Miall, A.D. (1996). The Geology of Fluvial Deposits: Sedimentary facies, Basin Analysis and Petroleum Geology: Springer, New York. 582pp.

Mitchum, R.M. Jr., Vail, P.R., Sangree, J.B. (1977). Seismic stratigraphy and global changes of sea level, part 6: stratigraphic interpretation of seismic reflection patterns in deposition sequences. In: C.E. Payton (Editor), Seismic Stratigraphy – Applications to Hydrocarbon Exploration: Am. Assoc. Pet. Geol. Mem., 26, 117-133.

Neal, A. (2004). Ground-penetrating radar and its use in sedimentology: principles, problems and progress. Earth-Science Reviews, 66, 261-330.

Neal, A. Grasmueck, M., McNeill, D.F., Viggiano, D.A. and Eberli, G.P. (2008). Full-Resolution 3D Radar Stratigraphy of Complex Oolitic Sedimentary Architecture: Miami Limestone, Florida, USA. Journal of Sedimentary Research, 78(9), 638-653.

Novo, A., Loreno, H., Rial, F.I., Pereira, M. and Solla, M. (2008). Ultra-dense Grid Strategies for 3D GPR in Archaeology. 12th International Conference on Ground Penetrating Radar, Birningham, UK. 5p.

Oldenborger, G.A., Schincaroil, R.A. and Mansinha, L. (2003). Radar determination of the spatial structure of hydraulic conductivity. Groundwater, 41 (1), 24-32.

Olsen, H. and Andreasen, F. (1995). Sedimentology and ground-penetrating radar characteristics of a Pleistocene sandur deposit. Sedimentary Geology, 99, 1-15.

Puckering, S.L., (2011) "Analysis of Bedrock Erosional Features in Ontario and Ohio: Improving Understanding of Subglacial Erosional Processes". [Unpublished M.Sc. thesis] McMaster University, Hamilton, Ontario. 183pp.

Reppert, P.M., Morgan, F.D. and Toksöz, M.N (2000). Dielectric constant determination using ground-penetrating radar reflection coefficients. Journal of Applied Geophysics, 43, 189-197.

Robinson, D.A., Binley, A., Crook, N., Day-Lewis, F.D., Ferre, T.P.A., Grauch, V.J.S., Knight, R., Knoll, M., Lakshmi, V., Miller, R., Jyquist, J., Pellerin, L., Singha, K. and Slater, L. (2008). Advancing process-based watershed hydrological research using near-surface geophysics: a vision for, and review of, electrical and magnetic geophysical methods. Hydrological Processes, 22, 1604-3635.

Russell, H.A.J., Sharpe, D.R. and Bajc, A.F. (2005) Sediment Architecture and Composition of the Waterloo Moraine, Southern Ontario: Emerging Insights. Illinois State Geological Survey, Three-Dimensional Geological Mapping for Groundwater Applications Workshops, 2005.

Slomka, J.M. (2011) "Sedimentary Architecture of Shallow and Deep Subsurface Quaternary Sediments, Southern Ontario". [Unpublished M.Sc. thesis] McMaster University, Hamilton, Ontario, 125p.

Sminchak, J.R, Dominic, D.F. and Ritzi, W. Jr. (1996) Indicator geostatistical analysis of sand interconnections within till. Groundwater, 34, 1125-1131.

Smith, D.G. and Jol, H.M. (1995). Ground-penetrating radar: antenna frequencies and maximum probable depths of penetration in Quaternary sediments. Journal of Applied Geophysics, 33, 93-100.

Stephens, M. (1994). Architectural Element Analysis within the Katenta Formation (Lower Jurassic) using Ground-probing Radar and Sedimentological Profiling, Southwestern Colorado. Sedimentary Geology, 90(3-4), 179-211.

Stephenson, D.A., Fleming, A.H. and Mickelson, D.M., (1988). Chapter 35: Glacial Deposits. Hydrogeology, The Geology of North America, Volume O-2. Boulder, Colorado: Geological Society of America.

Szerbiak, R.B,, McMechan, G.A., Corbeanu, R., Forster, C. and Snelgrove, S.H. (2001). 3-D Characterization of a clastic reservoir analog: From 3-D GPR data to a 3-D fluid permeability model. Geophysics, 66 (4), 1026-1037.

Van der Kruk, J., Slob, E.C. and Fokkema, J.T. (1999). Background of ground-penetrating radar measurements. Geologie en Mijnbouw, 77, 177-188.

Van Overmeeren, R.A. (1998). Radar facies of unconsolidated sediments in The Netherlands: A radar stratigraphy interpretation method for hydrogeology. Journal of Applied Geophysics, 40, 1-18.

Wills, M. (2008). Artificial Recharge Get Real. Water Wheel, 7(4), 38-39.

Wyatt, D.E., Waddell, M.G. and Sexton, B.G. (1996). Geophysics and Shallow Faults in Unconsolidated Sediments. Ground Water, 34(2), 326-334.

Xia, J., Franseen, E.K., Miller, R.D. and Weis, T.V. (2004) Application of deterministic deconvolution of ground-penetrating radar data in a study of carbonate strata. Journal of Applied Geophysics, in press.